A mineralogic approach to estimating the volume of dissolution, alteration, and unaltered residue from weathering of different provenance lithotypes

William Andrew Heins[1] and Latisha A Brengman[2]

[1]Getech Group plc
[2]University of Minnesota-Duluth, Department of Earth and Environmental Sciences
University of Minnesota-Duluth

August 24, 2023

Abstract

Evaluation of the approximate magnitude of the gross discrepancy between the volume of sediment produced on the hinterland and the volume deposited in the basin, over long time and length scales, is required to make source-to-sink sediment mass-balance calculations more accurate so that multiple sources for a single widespread stratigraphic unit, or bypass of the unit, might be more easily detected.

This paper outlines a method to characterize the sources of sediments, or provenance lithotypes, according to their relative ability to produce dissolved ions, clay minerals, and unaltered residue at different levels of weathering. Estimating the relative proportion of the hinterland that is dissolved supports mass-balance analysis comparing hinterland denudation with basinal deposition, whereas estimating the relative proportion of clay (both original clay, eroded from mudstone, for example, as well as newly created clay produced by weathering of feldspar) supports potential identification of multiple sediment sources. The method is illustrated with a practical example from the Bohemian Massif and documented with an Excel workbook.

This is a mineralogical approach based on mineral inventories of weathering profiles. Even if the prediction is necessarily uncertain because the mineralogical representation of the PLs are gross abstractions, the modelled transformation processes are crude cartoons, and the extent of transformation under different environmental conditions is wild speculation based on sparse examples, quantitative provenance analysis will be more accurate and more precise than it would be if dissolution and alteration were not explicitly accounted. There is ample opportunity for the community to improve the procedure!

A mineralogic approach to estimating the volume of dissolution, alteration, and unaltered residue from weathering of different provenance lithotypes

William A. Heins[1], Lathisha A. Brengman[2]

[1]Getech Group plc..

[2]Department of Earth and Environmental Science, University of Minnesota-Duluth.

Corresponding author: William A Heins (bill.heins@getech)

Key Points:

- A geochemical method is presented to estimate the fraction of minerals dissolved, altered, and residual after various weathering degrees.
- The method, calibrated to mineralogical observations, improves the accuracy and precision of source to sink mass-balance evaluations.
- The method is illustrated with an example and documented with an Excel workbook available for download.

Abstract

Evaluation of the approximate magnitude of the gross discrepancy between the volume of sediment produced on the hinterland and the volume deposited in the basin, over long time and length scales, is required to make source-to-sink sediment mass-balance calculations more accurate so that multiple sources for a single widespread stratigraphic unit, or bypass of the unit, might be more easily detected.

This paper outlines a method to characterize the sources of sediments, or provenance lithotypes, according to their relative ability to produce dissolved ions, clay minerals, and unaltered residue at different levels of weathering. Estimating the relative proportion of the hinterland that is dissolved supports mass-balance analysis comparing hinterland denudation with basinal deposition, whereas estimating the relative proportion of clay (both original clay, eroded from mudstone, for example, as well as newly created clay produced by weathering of feldspar) supports potential identification of multiple sediment sources. The method is illustrated with a practical example from the Bohemian Massif and documented with an Excel workbook.

This is a mineralogical approach based on mineral inventories of weathering profiles. Even if the prediction is necessarily uncertain because the mineralogical representation of the PLs are gross abstractions, the modelled transformation processes are crude cartoons, and the extent of transformation under different environmental conditions is wild speculation based on sparse examples, quantitative provenance analysis will be more accurate and more precise than it would be if dissolution and alteration were not explicitly accounted. There is ample opportunity for the community to improve the procedure!

Plain Language Summary

Estimating the fraction of material that is dissolved, altered to new materials, or remains as unaltered residue when rocks weather at the Earth's surface supports mass-balance analysis of sedimentary systems from source to sink. Mass-balance analysis help determine if sediments in a specific sediment body came from a single source or many sources, or if some sediments from potential sources has bypassed the deposit entirely. Knowing the source of sediment can help predict the physical properties of sediments even when they cannot be observed directly. This paper outlines a method for the estimation, provides a worked example from the Bohemian Massif, and supplies an Excel workbook to implement the estimation.

1 INTRODUCTION

1.1 Motivation

In resource exploration, it is often necessary to guess the physical properties of a sandstone body that cannot be directly observed, anything from the porosity and permeability of a potential hydrocarbon reservoir in a frontier basin with no wells for 100s of km (Ebner 2006), to the compressive strength of a potential bluestone deposit between quarries a few km apart (DePalma 2008). The financial stakes can be hundreds of millions of dollars for a deep-water well, or hundreds of dollars for a mining permit, but explorers need assurance that the potential resource is worth the expenditure. Often it is not necessary to be exactly right, but it is highly desirable not to be dramatically wrong.

One approach to physical-property estimation is forward modelling of sandstone diagenesis (Taylor et al. 2022), which combines an estimate of sand composition and texture at deposition, with the effective-stress/temperature/time history of the deposit after burial, to calculate the diagenetic processes and physical-property modifications that could have occurred. The estimate of sand composition and texture at deposition can be formally predicted with a tool like the Sand Generation and Evolution Model (SandGEM) (Heins & Kairo 2007, Kairo et al. 2010). Alternatively, the genetic principles of SandGEM can guide a systematic search for modern or ancient analogue sand(stone) with similar genetic context and similar burial-thermal history that could therefore be expected to demonstrate similar physical properties.

This paper outlines a procedure to characterize the sources of sediments, or provenance lithotypes (PL) according to their relative ability to produce dissolved ions, clay minerals, and unaltered residue at different levels of weathering, which is a useful step in estimating the depositional composition and texture of sediments that cannot be easily observed. Estimating the relative proportion of the hinterland that is dissolved supports mass-balance analysis comparing hinterland denudation with basinal deposition, whereas estimating the relative proportion of clay (both original clay, eroded from mudstone, for example, as well as newly created clay produced by weathering of feldspar) supports potential identification of multiple sediment sources (Heins 2023).

This is a mineralogical approach based on mineral inventories of weathering profiles that directly capture in situ interactions of the lithosphere, hydrosphere, and atmosphere. These methods have been previously outlined in Brengman et al. (2016), and first applied in public by Heins (2023). The calculations described in this paper are formalized in an Excel spreadsheet that is available for download as supplemental material. Although the approach might possibly aid more sophisticated evaluation of Sediment Routing Systems (Allen 2008, Allen 2017) or for Quantitative Provenance Analysis (Weltje and von Eynatten 2004, Weltje 2012, Caracciolo 2020), as discussed at the end of the paper, this is primarily a blunt tool to help make pragmatic exploration judgements that are unlikely to be dramatically wrong, because the judgements honour fundamental mineralogical and chemical principles.

1.2 Conceptual Framework

1.2.1 Raw Materials and Products

Not all the material removed from a source area will arrive in the sink as solids, and not all of the solids will be the same mineralogy as the original Provenance Lithotypes (PL) (Figure 1). Some fraction of the PL will have been dissolved (D) to ions, which leave the system in solution and cannot be tracked individually. Another fraction of the PL will be altered (A) to new minerals by the removal of the dissolved ions, for example plagioclase feldspars to various clay minerals. The residue (R) that has not been dissolved or altered consists of disintegrated original material with a different bulk mineralogy and chemical composition from the PL. The degree of alteration can be quantified by comparing the bulk chemical composition of the new minerals plus the unaltered residue to the bulk chemical composition of the original PL, for example using the Chemical Index of Alteration (CIA) introduced by Nesbitt & Young (1982). We do not advocate CIA for any other purpose than the conceptual comparison of parent material to daughter weathering products in the thought experiment where the entire volume of daughter products can be quantified; in practice it is rarely possible to ensure that a natural sample fully captures all daughter products (Weltje et al. 1998, Garzanti & Resentini 2016, Hatzenbühler et al. 2022).

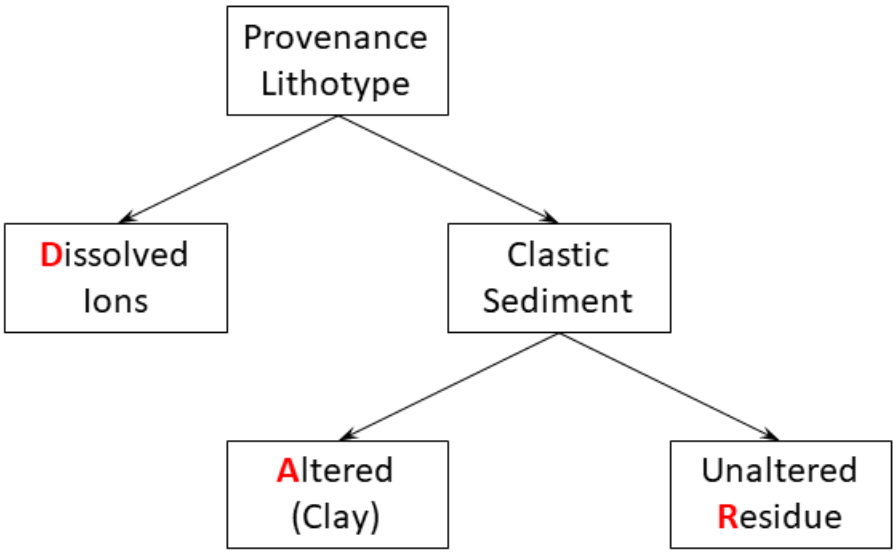

Figure 1– Partitioning of products from the breakdown of a single Provenance Lithotype

1.2.2 Procedure

We estimate the relative proportion of dissolved, altered, and residual material produced by weathering a defined roster of common rock types using geochemical mass balance. The procedure can be generalized to any provenance lithotype. We refer to the procedure by the acronym DARE (Dissolution, Alteration, and Residue Estimator).

1.2.3 Scale

The typical object of analysis will be several hundred meters to a few km of rock (102-103 m) removed from thousands to tens of thousands of square kilometers (103-104 km2) of landscape during hundreds of thousands to millions of years (105-106 years). Bookkeeping is done within a Lagrangian framework (Section 9.3 of Weltje 2012), in which we consider together all the residue, altered minerals, and dissolved ions that were derived from an originally contiguous volume of parent rock, regardless of where the individual bits have migrated in space. The altered and residual materials certainly will not all be deposited in the same place at the time (Castelltort & Van Den Driessche 2003, Allen 2008, Romans et al. 2016, Toby et al. 2019, Caracciolo 2020) because different parts of the landscape will produce sediments at different rates, the sediments will leave the landscape at different rates, and travel to the basin by different routes, and at different rates, according to the morphology of the landscape and the hydrodynamics of different kinds of particles; in the basin the material will be segregated into different depositional environments. Nevertheless, over the intended time and length scale, in many kinds of basins, a meaningful fraction of the original sediment generated on the hinterland will be deposited as sediment bodies large enough to serve as economically meaningful reservoirs (for hydrocarbons, or geothermal fluids, or captured carbon dioxide, for example): 102-103 m thick covering 103-104 km2. DARE is intended to address the approximate magnitude of the gross discrepancy between the volume of sediment produced on the hinterland and the volume deposited in the basin, to make mass-balance calculations more accurate so that multiple sources for a single deposit, or bypass of the deposit, might be more easily detected (Heins 2023). Application of this procedure to smaller spatial scales, or to shorter time scales, or to other analytic requirements may not produce meaningful results (Heins & Bailey 2020, see also the Discussion and Conclusion section).

1.2.4 Relative Uncertainty

The relative proportion of Dissolved (D), Altered (A), and Residual (R) components is one of the least uncertain elements in a sediment mass-balance analysis. D + A + R must add up to the total material removed from the landscape, which almost always is the most uncertain element. Imprecision in partitioning the denuded volume into the three elements for a given PL pales into insignificance in comparison to the uncertainty in defining the denuded volume and inaccuracy in quantifying it.

For example, in the study of Barnes & Heins (2007), which constitutes a well-constrained example, the uncertainty in the volume denuded from the Bolivian Andes during part of the Miocene encompassed three variables:

1. the size of the drainage area (somewhere between 100,000 and 153,000 km2);
2. the average rate of vertical incision (0.1-0.4 mm/year = km/Ma)
3. the duration of incision (2.1 ± 0.2 Ma)

The contrast between the smallest convolution (19,000 km3) and the largest convolution (141,000 km3) of these three factors is 7.4x.

By comparison, 1000 cm3 of fresh granodiorite weathered to its final, chemically stable, mineral assemblage would:

- dissolve 352 cm3

- alter 376 cm3 to clay
- retain 272 cm3 of unaltered residue (mostly quartz with traces of heavy minerals).

This represents a contrast between maximum and minimum values (no weathering vs maximal weathering) of 1.5x = 1000/(376+272) for the total mass of solid material, and 2.4x = (376+272)/272 for the proportion of altered material in the solids.

In most of the practical cases we have examined, the relative uncertainty in the denuded volume is even bigger than the special case of the Bolivian Andes, due to the uncertain location of ancient drainage divides (Markwick & Valdes 2004) and the inherent difficulty of converting imprecise point estimates of vertical incision into accurate rates of areal denudation (Barnes & Heins 2007, Sadler & Jerolmack 2014, Heins & Bailey, 2020)

The uncertainty in the solid yield and the fraction of alteration within the solids typically is even smaller than the granodiorite example above because the degree of alteration is rarely maximal and the PL assemblage tends to include (or even be dominated by) rocks that have a smaller content of labile minerals than granodiorite (for example quartzose sandstone).

Estimates of the relative proportion of different PL on the landscape are also uncertain, even on modern Earth (let alone projected into the past), given the vagaries of geologic mapping, especially at smaller scales (Dürr et al. 2005, Hartmann & Moosdorf 2012, Börker et al. 2018). Since the estimates for any single PL are reasonable and directionally correct, inaccuracies in the landscape-averaged values for D, A, and R will tend to be attenuated by the uncertainties in relative mix of all the PLs, rather than accentuated by that uncertainty.

1.3 Value of the Process

The values for D, A, and R calculated by the method reported below are not unreasonable (for example limestone can be dissolved almost completely at maximal alteration, quartz sandstone hardly at all) and directionally correct (for example gabbro produces more clay than granodiorite). At the same time, the values are bound to be wrong in detail because the mineralogical representation of the PLs are gross abstractions (Heins & Kairo 2007), the modelled alteration processes are crude cartoons (Velbel 1984), and the extent of alteration under different environmental conditions is wild speculation based on sparse examples (Nesbitt & Wilson 1992; Nesbitt & Markovics, 1997).

Nevertheless, using values calculated by this method in mass-balance calculations will yield better results than if dissolution and alteration were not accounted for, and the relative errors introduced will be very small compared to other uncertainties in the calculation (Heins 2023). Any of the specific factors presented in this paper easily can be modified by the interested user to reflect local conditions ± superior calibration data ± better reaction equations. We offer these values and this methodology as a starting point that can and should be improved by subsequent research.

2 PROCEDURE

2.1 Workflow

The general procedure to estimate the relative proportion of D, A, and R from a landscape consists of eight discrete steps, which will be presented in greater detail in subsequent sections of the paper. Any or all these steps can be improved or refined by additional investigation by the interested reader.

1. Specify a short list of provenance lithotypes that can reasonably represent an adequate fraction of the hinterland.
2. Specify a short list of idealized minerals and glasses that can reasonably represent an adequate fraction of the PL.
3. Assign an idealized mineralogic composition for each PL from the list of minerals.
4. Identify the daughter weathering products for each of the minerals.
5. Establish a small number of discrete, qualitative, weathering steps between the end members of "no alteration" to "maximum possible alteration".
6. Quantify the volumetric proportion of parent mineral altered (alteration index) at each step, and the volume reduction from the parent to the daughter.
7. Calculate the volume of remaining altered and unaltered material for each mineral (or glass), at each weathering step.
8. Integrate the values for each mineral (or glass), at each weathering step, weighted by the composition of each provenance lithotype.

2.1.1 Specify Provenance Lithotypes

A Provenance Lithotype encompasses all rocks of similar mineralogy and texture that tend to generate the same volume and character (mineralogy and texture) of sediments when subjected to a given level of alteration (Heins & Kairo 2007). Heins & Kairo 2007 identified a global list of 21 different PL (Table 1). Dürr et al. 2005 suggest a global list of 15 types (including water and ice). Hartmann & Moosdorf 2012 suggest a high-level division of 16 classes (including unconsolidated sediments) with two optional modifiers with 12 and 14 values, respectively. Börker et al. 2018 expand on the recognition of Hartmann & Moosdorf 2012 that unconsolidated sediments are in many cases the most important PL and refines the classification of those deposits.

For this paper we adopt the convention of Heins & Kairo 2007, but practical experience shows this list is deficient in the roster of metamorphic rocks, which should be expanded to address the wide range of metamorphic textures and mineralogies among rocks typically lumped together in "Precambrian shields" or other poorly resolved areas of quartzo-feldspathic crystalline basement.

The roster of sedimentary rocks is probably adequate, but care must be taken when inferring the relative abundance of "sandstone", "mudstone", and "carbonate" in mapped sedimentary units. Very often the relative abundance of fine-grained rocks is under-reported or under-appreciated in map units designated as "sand" or "sandstone", and the carbonate content of "shales" or "mudstones" is often underappreciated: famous mudrocks like the Posidonienschiefer of Germany or the Eagle Ford Shale of Texas are one-third to two-thirds carbonate.

Table 1– Example List of Provenance Lithotypes

Code	Clan	Variant	Variety	Comment
P1	Plutonic	Ultrabasic		
P2	Plutonic	Basic	Gabbro	Na-plagioclase dominant
P3	Plutonic	Basic	Diorite	Ca-plagioclase dominant
P4	Plutonic	Intermediate		
P5	Plutonic	Silicic		
P6	Plutonic	Sodic	Anorthosite	
P7	Plutonic	Potassic	Syenite	
V1	Volcanic	Basic		
V2	Volcanic	Intermediate		
V3	Volcanic	Silicic		
S1	Sedimentary	Sandstone	Quartz-rich	
S2	Sedimentary	Sandstone	Feldspar-rich	
S3	Sedimentary	Sandstone	Lithic-rich	
S4	Sedimentary	Mudstone		
S5	Sedimentary	Carbonate		
M1	Metamorphic	Metasandstone		
M2	Metamorphic	Slate		
M3	Metamorphic	Metacarbonate		
M4	Metamorphic	Schist/phyllite		
M5	Metamorphic	Gneiss	Plagioclase-rich	
M6	Metamorphic	Gneiss	K-feldspar-rich	

2.1.2 Specify Minerals

The mineral list must be long enough to capture the essential weathering behavior of all the PLs, but short enough to be tractable (Table 2). Whole categories of minerals like pyroxenes, amphiboles, micas, and clays are necessarily collapsed into one or a few representatives that stand in as idealized abstractions for the broader category to simplify the analysis. Especially for the clays we acknowledge that we have grossly oversimplified to make computations tractable. Each mineral in the table has been abstracted to typical chemistry (Stoch & Sikora 1976, Schroeder et al. 2000, van der Weijden & Pacheco 2003) that can be used for quantitative weathering calculations, and still plausibly stand in for the range of variation in nature.

The minerals in Table 2 are listed approximately in their order of weathering susceptibility as integrated from Nesbitt & Wilson 1992, Lasaga et al. 1994, Nesbitt & Markovics 1997, Railsback 2007, and Brantley 2008.

The list of Table 2 and the specified compositions have the added advantage that they provide suitable targets for the linear algebra method (Nesbitt et al. 1996, Nesbitt & Markovics 1997) for inverting modal mineralogy from major oxide compositions of PL. Apatite is listed among the minerals primarily to account for P_2O_5; apatite typically is not abundant enough to make any difference in mass balance calculations. Garnets are excluded from the list because they are rarely abundant enough in rocks to make a discernible difference in mass balance calculations. The molar mass reported in Table 2 is calculated from the given chemical formula. The molar volume is calculated from the reported molar

mass and the reported typical density. References are provided for both the formulae and the densities.

2.1.3 Assign Minerals to Provenance Lithotypes

The minerals listed in Table 2 are sufficient to describe the provenance lithotypes listed in Table 1 completely, as outlined in Table 3 and Table 4. Typical major oxide compositions of the Provenance Lithotypes from Table 1 are provided in Table 5 (after Heins & Kairo 2007). The reported mineralogic and chemical compositions are intended only as convenient abstractions for a typical representative of each rock type to ease subsequent calculations. The interested reader is encouraged to use different values that may more accurately represent specific circumstances.

2.1.4 Weathering Products of Minerals

The rock-forming minerals or glasses of Table 2 lose mass and volume as they alter into another mineral (usually a clay) or dissolve completely. The daughter products and associated fractional volume loss during alteration are calculated in Table 6, for minerals, and in Table 7, for glasses. Apatite and calcite are not included in the list because they are considered to dissolve completely without solid daughter products; kaolinite, quartz, rutile, and hematite are not included because they are considered fully resistant to alteration (although these assumptions are not strictly true in real life). Treating apatite as a highly labile minerals rests on the very high dissolution rates reported by Brantley 2008, Figure 5.1. Obviously, apatite is common as a detrital component in sandstones, and even has special value as a provenance indicator (O'Sullivan et al. 2020). It would be equally legitimate to include apatite among the refractory minerals, like quartz, that are assumed not to dissolve at all. Both decisions have no practical impact as apatite is rarely if ever abundant enough in the PL to make a discernible difference in a mass-balance calculation; apatite is included in the mineral list primarily to accommodate P2O5 when inverting oxide geochemistry to mineralogy.

The parent minerals or glasses and daughter weathering products present in Table 6 are idealized end members of illustrative sequences that can only vaguely approximate the complexity of nature. The precise definitions of the daughter weathering products are chosen to simplify calculations. The interested reader is encouraged to use different values that may more accurately represent specific circumstances.

Table 2 – Example List of Minerals and Glasses

Mineral or Glass	Representative Chemical Formula	Molar mass (g)	Typical Density (g/cm^3)	Molar volume (cm^3)	Composition Reference	Density Reference
Apatite	$(CaO)_5(PO_4)_3$	565.3	3.20	176.7	1	1
Calcite	$CaCO_3$	100.1	2.71	36.9	1	1
Pyroxene	$CaMg_{0.7}Fe_{0.3}Al_{0.2}Si_{1.8}O_{5.9}$	224.2	3.50	64.1	2	1
Plagioclase (An_{100})	$CaAl_2Si_2O_8$	278.2	2.76	100.8	2	1
Olivine	$Mg_{1.5}Fe_{0.5}SiO_4$	156.5	3.51	44.5	2	1
Basaltic glass	same as V1 (**Error! Reference source not found.**) major oxide wt%		2.77			3
Andesitic glass	same as V2 (**Error! Reference source not found.**) major oxide wt%		2.47			3
Rhyolitic glass	same as V3 (**Error! Reference source not found.**) major oxide wt%		2.37			3
Biotite	$KMg_3AlSi_3O_{10}(OH)_2$	417.3	3.00	139.1	4	1
Hornblende	$Na_{0.45}Ca_{1.90}Mg_{2.33}Fe^{2+}_{1.98}Al_{0.80}Si_{6.53}Al_{1.45}Ti_{0.02}O_{22}(OH)_2$	884.8	3.24	273.5	5	1
Plagioclase (An_{70})	$Na_{0.3}Ca_{0.7}Al_{1.7}Si_{2.3}O_8$	273.4	2.72	100.5	2	1
Plagioclase (An_0)	$NaAlSi_3O_8$	262.2	2.63	99.7	2	1
K-feldspar	$KAlSi_3O_8$	278.3	2.55	109.1	1	1
Muscovite	$KAl_2Si_3AlO_{10}(OH)_2$	398.3	2.83	141.0	4	1
Vermiculite	$Mg_{0.35}Fe_{0.3}Al_2Si_{3.6}O_{11}$	356.3	2.40	148.5	4	1
Illite	$K_{0.75}Al_{2.75}Si_{3.25}O_{10}(OH)_2$	388.8	2.75	141.4	4	1
Kaolinite	$Al_2Si_2O_5(OH)_4$	258.2	2.60	99.3	4	1
Quartz	SiO_2	60.1	2.33	25.8	1	1
Rutile	TiO_2	79.9	4.90	16.3	1	1
Hematite	Fe_2O_3	159.7	5.26	30.4	1	1

References:

1. Phillips & Griffin 1981
2. van der Weijden & Pacheco 2003
3. Wohletz & Heiken 1992

4. Stoch & Sikora 1976
5. Schroeder *et al.* 2000

Table 3 – Typical Mineralogy of Plutonic and Volcanic Provenance Lithotypes

	P1	**P2**	**P3**	**P4**	**P5**	**P6**	**P7**	**V1**	**V2**	**V3**
Apatite	0.010	0.005	0.016	0.023	0.010	0.000	0.020	0.004	0.003	0.001
Calcite	0.000	0.000	0.000	0.000	0.000	0.000	0.000	0.000	0.000	0.000
Pyroxene	0.263	0.198	0.189	0.000	0.000	0.050	0.000	0.132	0.000	0.000
Plagioclase (An_{100})	0.120	0.615	0.606	0.000	0.000	0.000	0.000	0.000	0.000	0.000
Olivine	0.548	0.151	0.167	0.000	0.000	0.040	0.000	0.117	0.000	0.000
Basaltic glass	0.000	0.000	0.000	0.000	0.000	0.000	0.000	0.300	0.000	0.000
Andesitic glass	0.000	0.000	0.000	0.000	0.000	0.000	0.000	0.000	0.300	0.000
Rhyolitic glass	0.000	0.000	0.000	0.000	0.000	0.000	0.000	0.000	0.000	0.300
Biotite	0.000	0.000	0.000	0.056	0.070	0.000	0.080	0.000	0.011	0.026
Hornblende	0.000	0.000	0.000	0.024	0.000	0.000	0.000	0.000	0.092	0.000
Plagioclase (An_{70})	0.000	0.000	0.000	0.153	0.150	0.900	0.000	0.000	0.187	0.037
Plagioclase (An_{0})	0.000	0.000	0.000	0.319	0.260	0.000	0.150	0.262	0.211	0.185
K-feldspar	0.000	0.000	0.000	0.175	0.150	0.000	0.680	0.163	0.054	0.230
Muscovite	0.000	0.000	0.000	0.000	0.000	0.000	0.000	0.000	0.000	0.000
Vermiculite	0.000	0.000	0.000	0.000	0.000	0.000	0.000	0.000	0.000	0.000
Illite	0.000	0.000	0.000	0.000	0.000	0.000	0.000	0.000	0.000	0.000
Kaolinite	0.000	0.000	0.000	0.000	0.000	0.000	0.000	0.000	0.000	0.000
Quartz	0.000	0.000	0.000	0.247	0.350	0.000	0.050	0.000	0.142	0.220
Rutile	0.034	0.016	0.015	0.000	0.000	0.010	0.000	0.011	0.000	0.000
Hematite	0.026	0.015	0.006	0.001	0.010	0.000	0.020	0.011	0.000	0.000

Table 4 – Typical Mineralogy of Sedimentary and Metamorphic Provenance Lithotypes

	S1	**S2**	**S3**	**S4**	**S5**	**M1**	**M2**	**M3**	**M4**	**M5**	**M6**
Apatite	0.000	0.000	0.000	0.000	0.000	0.000	0.000	0.000	0.000	0.000	0.000
Calcite	0.010	0.050	0.100	0.045	0.750	0.000	0.030	0.750	0.000	0.000	0.000
Pyroxene	0.000	0.000	0.000	0.000	0.000	0.000	0.000	0.000	0.000	0.000	0.000
Plagioclase (An_{100})	0.000	0.000	0.000	0.000	0.000	0.000	0.000	0.000	0.000	0.000	0.000
Olivine	0.000	0.000	0.000	0.000	0.000	0.000	0.000	0.000	0.000	0.000	0.000
Basaltic glass	0.000	0.000	0.000	0.000	0.000	0.000	0.000	0.000	0.000	0.000	0.000
Andesitic glass	0.000	0.000	0.000	0.000	0.000	0.000	0.000	0.000	0.000	0.000	0.000
Rhyolitic glass	0.000	0.000	0.000	0.000	0.000	0.000	0.000	0.000	0.000	0.000	0.000
Biotite	0.013	0.050	0.100	0.000	0.000	0.050	0.000	0.000	0.325	0.006	0.060
Hornblende	0.000	0.000	0.000	0.000	0.000	0.000	0.000	0.000	0.000	0.000	0.000
Plagioclase (An_{70})	0.010	0.094	0.063	0.000	0.010	0.000	0.000	0.010	0.000	0.000	0.004
Plagioclase (An_{0})	0.035	0.094	0.063	0.010	0.010	0.150	0.030	0.010	0.050	0.325	0.083
K-feldspar	0.045	0.188	0.125	0.030	0.010	0.150	0.010	0.010	0.050	0.175	0.413
Muscovite	0.000	0.000	0.000	0.000	0.000	0.000	0.000	0.000	0.325	0.095	0.040
Vermiculite	0.000	0.000	0.000	0.183	0.000	0.000	0.210	0.000	0.000	0.000	0.000
Illite	0.000	0.000	0.000	0.366	0.000	0.000	0.300	0.000	0.000	0.000	0.000
Kaolinite	0.000	0.000	0.000	0.061	0.050	0.000	0.100	0.050	0.000	0.000	0.000
Quartz	0.875	0.475	0.450	0.300	0.150	0.550	0.300	0.150	0.050	0.250	0.250
Rutile	0.013	0.050	0.100	0.005	0.020	0.050	0.010	0.010	0.180	0.140	0.140
Hematite	0.000	0.000	0.000	0.000	0.000	0.050	0.010	0.010	0.020	0.010	0.010

Table 5 – Major Element Oxide Composition of Provenance Lithotypes

PL	SiO2	TiO2	Al203	Fe2O3	FeO	MnO	MgO	CaO	Na2O	K2O	H2O	P2O5	
P1	43.54	0.81	3.99	2.51	9.84	0.21	34.02	3.46	0.56	0.25	0.76	0.05	Table 48, “Peridotite”
P2	48.36	1.32	16.81	2.55	7.92	0.18	8.06	11.07	2.26	0.56	0.64	0.24	Table 47, “Gabbros”
P3	51.86	1.50	16.40	2.73	6.97	0.18	6.12	8.40	3.36	1.33	0.80	0.35	Table 46, “Diorites”
P4	66.80	0.57	15.66	1.33	2.59	0.07	1.57	3.56	3.84	3.07	0.65	0.21	Table 45, “Granodiorites”
P5	72.08	0.37	13.86	0.86	1.67	0.06	0.52	1.33	3.08	5.46	0.53	0.18	Table 45, “Granites”
P6	54.54	0.52	25.72	0.83	1.46	0.02	0.83	9.62	4.66	1.06	0.63	0.11	Table 48, “Anorthosites”
P7	59.41	0.83	17.12	2.19	2.83	0.08	2.02	4.06	3.92	6.53	0.63	0.38	Table 46, “Syenites”
V1	50.83	2.03	14.07	2.88	9.00	0.18	6.34	10.42	2.23	0.82	0.91	0.23	Table 47, “Tholeiitic basalts"
V2	54.20	1.31	17.17	3.48	5.49	0.15	4.36	7.92	3.67	1.11	0.86	0.28	Table 46, “Andesites”
V3	73.66	0.22	13.45	1.25	0.75	0.03	0.32	1.13	2.99	5.35	0.78	0.07	Table 45, “Rhyolites”
S1	78.70	0.25	4.80	1.10	0.30	0.03	1.20	5.50	0.45	0.30	1.30	0.08	Table 87, “Sandstones”
S2	70.00	0.58	8.20	2.50	1.50	0.06	1.90	4.30	0.58	2.10	3.00	0.10	Table 87, “Sandstones from platforms"
S3	66.70	0.60	13.50	1.60	3.50	0.10	2.10	2.50	2.90	2.00	2.40	0.20	Table 87, “Graywackes”
S4	58.90	0.78	16.70	2.80	3.70	0.09	2.60	2.20	1.60	3.60	5.00	0.16	Table 87, “Shales mainly from geosynclines"
S5	8.20	0.00	2.20	1.00	0.68	0.07	7.70	40.50	0.00	0.00	0.00	0.07	Table 87, “Carbonate rocks"
M1	78.70	0.25	4.80	1.10	0.30	0.03	1.20	5.50	0.45	0.30	1.30	0.08	Table 87, “Sandstones”
M2	58.90	0.78	16.70	2.80	3.70	0.09	2.60	2.20	1.60	3.60	5.00	0.16	Table 87, “Shales mainly from geosynclines"
M3	8.20	0.00	2.20	1.00	0.68	0.07	7.70	40.50	0.00	0.00	0.00	0.07	Table 87, “Carbonate rocks"
M4	62.00	1.00	19.00	2.60	4.70	0.10	2.80	1.50	2.00	3.90	0.00	0.20	Table 95, mean of "Phyllite" & "Mica schists"
M5	50.30	1.60	15.70	3.60	7.80	0.20	7.00	9.50	2.90	1.10	0.00	0.30	Table 95, “Amphibolites”
M6	70.70	0.50	14.50	1.60	2.00	0.10	1.20	2.20	3.20	3.80	0.00	0.20	Table 95, “Quartzofeldspathic gneisses"

Reference – Clark 1982

Table 6 – Parents & Daughters, Minerals

Parent Mineral or Glass	Ultimate Daughter	Molar volume of parent (cm^3)	Moles of parent to make 1 mole daughter (#/#)	Volume of parent to make 1 mole daughter (cm^3)	Molar volume of daughter (cm^3)	Fractional Volume reduction	Stoichiometry Reference
Pyroxene	Vermiculite	64.1	10.2	653.3	148.5	0.773	1
Plagioclase (An_{100})	Kaolinite	100.8	1	100.8	99.3	0.015	1
Olivine	Hematite	44.5	4	178.2	30.4	0.830	1
Biotite	Kaolinite	139.1	1	139.1	99.3	0.286	2
Hornblende	Kaolinite	273.5	0.98	268.1	99.3	0.630	3
Plagioclase (An_{70})	Kaolinite	100.5	1.7	170.8	99.3	0.419	1
Plagioclase (An_0)	Kaolinite	99.7	2	199.4	99.3	0.502	1
K-feldspar	Illite	109.1	2	218.3	138.4	0.366	4
Muscovite	Kaolinite	141.0	1.33	188.0	99.3	0.472	2
Vermiculite	Kaolinite	148.5	2	296.9	99.3	0.666	3
Illite	Kaolinite	141.4	0.93	131.5	99.3	0.245	5

References:

1. van der Weijden & Pacheco 2003
2. Stoch & Sikora 1976
3. Schroeder *et al.* 2000
4. Yuan *et al.* 2019
5. Jin *et al.* 2010

Table 7 – Parents & Daughters, Glass

Parent Glass	Density (g cm^{-3})	Mass of 100 cm^3 of glass (g)	Al_2O_3 fraction (wt/wt)	Mass of Al_2O_3 in 100 cm^3 of glass (g)	Molar weight of Al_2O_3 (g/mol)	Moles of Al_2O_3 in 100 cm^3 of glass	Moles of kaolinite produced by 100 cm^3 of glass	Molar weight of kaolinite (g/mol)	Mass of kaolinite produced by 100 cm^3 of glass (g)	Density of kaolinite (g cm^{-3})	Volume of kaolinite produced by 100 cm^3 of glass (cm^3)	Fractional Volume reduction
Basaltic	2.772	277.2	0.1599	44.32	101.96	0.435	0.435	258.16	112.23	2.60	43.16	0.568
Andesitic	2.474	247.4	0.1722	42.60	101.96	0.418	0.418	258.16	107.87	2.60	41.49	0.585
Rhyolitic	2.370	237.0	0.1353	32.07	101.96	0.314	0.314	258.16	81.19	2.60	31.23	0.688

Glass Al_2O_3 content and density reference: Wohletz & Heiken 1992, Tables B.1 and B.3

2.1.5 Qualitative Weathering Steps

We follow the example of Nesbitt & Wilson 1992 in identifying four qualitative weathering categories, as outlined in Table 8: incipient, intermediate, advanced, and extreme. Each progressively higher step implies a greater alteration of the original PL, with a corresponding reduction in volume and increase in the relative proportion of altered material to unaltered residue.

The categories divide up the total possible range of outcomes, from no modification to complete modification. In the absence of suitable (Weltje et al. 1998, Garzanti & Resentini 2016, Hatzenbühler et al. 2022) residual material to estimate a Chemical Index of Alteration associated with the weathering environment, the relevant step for a given environmental context can be evaluated using the logic for the "Transport Modification Potential" node of the Sand Generation and Evolution Model (Heins & Kairo 2007): weathering pathways predicted to produce highly quartzose (Q80-90) sand from landscapes dominated by quartzo-feldspathic crystalline basement would correspond approximately to "Advanced", whereas weathering pathways predicted to produce pure quartz sand (Q100) would correspond approximately to "Extreme".

Table 8 – Weathering Steps

Qualitative Weathering State	**Description**	**Approximate Quantitative Range of Chemical Index of Alteration (CIA)**			
		Mafic		*Felsic*	
Incipient	Primary minerals like quartz, feldspar, mica, amphibole, *etc.* dominate	42	50	50	73
Intermediate	Primary minerals that can alter have mostly been replaced by secondary alteration products like smectite, vermiculite, chlorite, and illite	50	91	73	86
Advanced	Secondary minerals have mostly been replaced by kaolinite and oxides/oxyhydroxides	91	94	86	94
Extreme	No clay minerals remain, all alterable material has been reduced to oxides, oxyhydroxides, and hydroxides of Fe, Al, and Ti	94	100	94	100

2.1.6 Quantitative Mineral Alterations

At each weathering step from incipient to extreme, some fraction of the original parent material and/or the alteration products of the previous step will be altered. The fraction for each mineral can be roughly estimated using examples from observed weathering of the Baynton Basalt (Nesbitt & Wilson 1992, their Figure 2) and the Toorongo Granodiorite (Nesbitt & Markovics 1997, their Table 3). Between them, these two examples cover most of the minerals of Table 2 in this paper, as summarized in Table 9 and Table 10 below.

Table 11 summarizes the fractional volume altered (also known as the alteration index), compared to the unaltered volume, by each parent mineral at each weathering step. The values in Table 11 are derived according to the following principals:

- the values for apatite and calcite assume that these two minerals are completely dissolved with even incipient weathering;
- the values for Pyroxene, Plagioclase (An100), Olivine, and Basaltic Glass are taken directly from Table 9;
- the values for Andesitic and Rhyolitic glasses are proportional reductions from the values for Basaltic glass;
- the values for Biotite, Hornblende, Plagioclase (An70), Plagioclase (An0), and Kspar are taken directly from Table 10;
- the values for Muscovite, Vermiculite, and Illite are proportional reductions from the values for Kspar.

The values in Table 11 are intended to be directionally correct and suitable for subsequent calculations. Although they are reported to 3 decimal places, they represent highly idealized outcomes that in the end are essentially qualitative.

Table 9 – Progressive Alteration of Baynton Basalt
(Nesbitt & Wilson 1992 Figure 2)

Mineralogy	**Samples (least to most weathered)**				
	A-1 *Starting bulk volume %*	A-2 *Remaining bulk volume %*	A-4 *Remaining bulk volume %*	A-6 *Remaining bulk volume %*	A-9 *Remaining bulk volume %*
Plagioclase	39	15	0	0	0
Glass	30	25	2	0	0
Olivine	11	5	0	0	0
Pyroxene	15	5	2	0	0
Fraction of Mineral in Parent Altered at Each Step					
Plagioclase	0.000	0.615	1.000	1.000	1.000
Glass	0.000	0.167	0.933	1.000	1.000
Olivine	0.000	0.545	1.000	1.000	1.000
Pyroxene	0.000	0.667	0.867	1.000	1.000

Table 10 – Progressive Alteration of Toorongo Granodiorite
(Nesbitt & Markovics 1997 Table 3)

Mineralogy	**Samples (least to most weathered)**				
	1 *Starting bulk volume %*	4 *Remaining bulk volume %*	9 *Remaining bulk volume %*	13 *Remaining bulk volume %*	15 *Remaining bulk volume %*
Albite	29.6	28	21.8	2.8	0
Anorthite	17.3	15.8	6.9	1	0
K-feldspar *	9.6	9.2	8.7	4	0
Biotite + Chlorite	13.6	12.4	2.3	0	0
Hornblende	3.4	3.1	0.6	0	0
Fraction of Mineral in Parent Altered at Each Step					
Albite	0.000	0.054	0.264	0.905	1.000
Anorthite	0.000	0.087	0.601	0.942	1.000
K-feldspar	0.000	0.042	0.094	0.583	1.000
Biotite + Chlorite	0.000	0.088	0.831	1.000	1.000
Hornblende	0.000	0.088	0.824	1.000	1.000

* K-felspar value for sample 13 is the average of 13 and 14

Table 11 – Fraction of Each Parent Mineral Altered at Each Weathering Step

Minerals		**Alteration Index**				**Maximum Volume Reduction**
Parent	*Daughter*	*Incipient*	*Intermediate*	*Advanced*	*Extreme*	
Apatite	Solution	1.000	1.000	1.000	1.000	1.000
Calcite	Solution	1.000	1.000	1.000	1.000	1.000
Pyroxene	Vermiculite	0.667	0.867	1.000	1.000	0.773
Plagioclase (An_{100})	Kaolinite	0.615	1.000	1.000	1.000	0.015
Olivine	Hematite	0.545	1.000	1.000	1.000	0.830
Basaltic glass	Kaolinite	0.167	0.933	1.000	1.000	0.568
Andesitic glass	Kaolinite	0.143	0.800	1.000	1.000	0.585
Rhyolitic glass	Kaolinite	0.125	0.700	1.000	1.000	0.688
Biotite	Kaolinite	0.088	0.831	1.000	1.000	0.286
Hornblende	Kaolinite	0.088	0.824	1.000	1.000	0.630
Plagioclase (An_{70})	Kaolinite	0.087	0.601	0.942	1.000	0.419
Plagioclase (An_{0})	Kaolinite	0.054	0.264	0.905	1.000	0.502
K-feldspar	Illite	0.042	0.094	0.583	1.000	0.366
Muscovite	Kaolinite	0.021	0.063	0.438	1.000	0.472
Vermiculite	Kaolinite	0.017	0.056	0.438	1.000	0.666
Illite	Kaolinite	0.013	0.051	0.438	1.000	0.245
Kaolinite	Kaolinite	0.000	0.000	0.000	0.000	0.000
Quartz	Quartz	0.000	0.000	0.000	0.000	0.000
Rutile	Rutile	0.000	0.000	0.000	0.000	0.000
Hematite	Hematite	0.000	0.000	0.000	0.000	0.000

Please refer to the text for the derivation of the alteration indices.

2.2 Integrated Alteration and Volume Reduction by Provenance Lithotype and Weathering Step

Table 12 summarizes the procedure to integrate parent mineral alteration and daughter-mineral volume reduction to calculate the volume of dissolved, altered, and residual material, as well as the composition of the derived sediment, for a particular PL at a particular weathering step. The following sections describe how the values in each column of the table are calculated.

2.2.1 PL Composition

The column "PL Composition" comes from Table 3 (for igneous rocks) or Table 4 (for sedimentary or metamorphic rocks. This example uses the composition of P4, plutonic intermediate (granodiorite). The values in this column are the proportions of the original volume of each mineral to the original volume of the whole rock before weathering (v0/v0). The values do not depend on the weathering step.

2.2.2 Alteration Index

The column "Alteration Index" comes from Table 11. This example uses the values for the "Intermediate" weathering step. Each value represents the fraction of the original volume of parent mineral that will be altered to something else (dissolved ions and daughter mineral). The values do not depend on the PL, only on the weathering step.

2.2.3 Volume Reduction

The column "Volume Reduction" comes from Table 6 (for minerals) or Table 7 (for volcanic glass). This column is the same regardless of the PL or the weathering step. These values represent the volume fraction of original parent mineral lost during the creation of the daughter mineral.

2.2.4 Parent Remaining

The column "Parent Remaining" is equal to "PL Composition" x (1-"Alteration Index"). It is the volume of parent mineral left after alteration (v1), compared to the original volume of that mineral (v0). If there was no Parent present in the original rock, the value will be zero, regardless of the Alteration Index. The sum of all the values in this column represents the volumetric proportion of Residual, unaltered material (R) at the conclusion of weathering, compared to the original volume of rock.

2.2.5 Daughter Produced

The column "Daughter Produced" is equal to "PL Composition" x "Alteration Index" x (1-"Volume Reduction"). It is the volume of daughter mineral produced by the alteration, compared to the volume of the original parent that was altered. The sum of all the values in this column represents the volumetric proportion of Altered material (A) at the conclusion of weathering, compared to the original volume of rock.

2.2.6 Parent Dissolved

The column “Parent Dissolved” is equal to “PL Composition” – “Parent Remaining” – “Daughter Produced”. The sum of all the values in this column represents the volumetric proportion of Dissolved material (D) at the conclusion of weathering, compared to the original volume of rock. The sum of D + A + R must equal 1.

2.2.7 Sediment Composition

The column “Sediment Composition” is reported with respect to the clastic sediments (A + R) produced by weathering; it is the volumetric proportion of each component in the generated sediment.

- The values for all lines from “Carbonates” through “K-feldspar” are equal to the value for that line in “Parent Remaining” divided by the sum of the columns “Parent Remaining” and “Daughter Produced”.
- The values for the clay-mineral line “Vermiculite”, represents the sum of “Parent Remaining” for “Vermiculite” plus the “Daughter Produced” for “Pyroxene”, divided by the sum of the columns “Parent Remaining” and “Daughter Produced”.
- The values for the clay-mineral line “Illite” represents the sum of “Parent Remaining” for “Illite” plus the “Daughter Produced” for “K-feldspar”, divided by the sum of the columns “Parent Remaining” and “Daughter Produced”.
- The values for the clay-mineral line “Kaolinite” represents the sum of “Parent Remaining” for “Kaolinite” plus the sum of “Daughter Produced” for the three volcanic glasses, the two micas, “Hornblende”, the three plagioclase feldspars, and the two other clays, divided by the sum of the columns “Parent Remaining” and “Daughter Produced”.

The sum of the “Sediment Composition” must equal 1.

Table 12 -- Integrated Calculation of Dissolved, Altered, and Residual Volumes for One Provenance Lithotype (P4) at One Weathering Step (Intermediate)

Table 12 -- Integrated Calculation of Dissolved, Altered, and Residual Volumes for One Provenance Lithotype (P4) at One Weathering Step (Intermediate)

Minerals		**PL composition**	**Alteration Index**	**Volume Reduction**	**Parent Remaining**	**Daughter Produced**	**Parent Dissolved**	**Sediment Composition**
Parent	*Daughter*	(v_0/v_0)	(v_0/v_0)	(v_1/v_0)	(v_1/v_0)	(v_1/v_0)	(v_0/v_0)	(v_1/v_1)
Apatite	Solution	0.023	1.000	1.000	0.000	0.000	0.023	0.000
Calcite	Solution	0.000	1.000	1.000	0.000	0.000	0.000	0.000
Pyroxene	Vermiculite	0.000	0.867	0.773	0.000	0.000	0.000	0.000
Plagioclase (An_{100})	Kaolinite	0.000	1.000	0.015	0.000	0.000	0.000	0.000
Olivine	Hematite	0.000	1.000	0.830	0.000	0.000	0.000	0.000
Basaltic glass	Kaolinite	0.000	1.000	0.568	0.000	0.000	0.000	0.000
Andesitic glass	Kaolinite	0.000	1.000	0.585	0.000	0.000	0.000	0.000
Rhyolitic glass	Kaolinite	0.000	1.000	0.688	0.000	0.000	0.000	0.000
Biotite	Kaolinite	0.056	0.831	0.286	0.009	0.033	0.013	0.011
Hornblende	Kaolinite	0.024	0.824	0.630	0.004	0.007	0.012	0.005
Plagioclase (An_{70})	Kaolinite	0.153	0.601	0.419	0.061	0.053	0.039	0.071
Plagioclase (An_0)	Kaolinite	0.319	0.264	0.502	0.235	0.042	0.042	0.272
K-feldspar	Illite	0.175	0.094	0.366	0.159	0.010	0.006	0.184
Muscovite	Kaolinite	0.000	0.063	0.472	0.000	0.000	0.000	0.000
Vermiculite	Kaolinite	0.000	0.056	0.666	0.000	0.000	0.000	0.000
Illite	Kaolinite	0.000	0.051	0.245	0.000	0.000	0.000	0.012
Kaolinite	Kaolinite	0.000	0.000	0.000	0.000	0.000	0.000	0.158
Quartz	Quartz	0.247	0.000	0.000	0.247	0.000	0.000	0.286
Rutile	Rutile	0.000	0.000	0.000	0.000	0.000	0.000	0.000
Hematite	Hematite	0.001	0.000	0.000	0.001	0.000	0.000	0.001

3 Results

We have repeated the same kind of calculation reported in Table 12 for all the PL and all the weathering steps. The results are reported in Table 13, Table 14, Table 15, and Table 16. Each table summarize the results for every PL under Incipient, Intermediate, Advanced, and Extreme weathering, respectively. The tables report the partitioning of the total volume in two ways: among Dissolved, Altered, and Residual; and among Quartz, Feldspar, Clay, and Other constituents.

The values in these tables are intended to be directionally correct and convenient for sediment budget or mass balance calculations. Although they are reported to 3 decimal places, they represent highly idealized outcomes that are essentially qualitative and should be considered as gross approximations within a wide range of variation.

Table 13 – Summary Results for All PL under Incipient Weathering

PL	Short Name	Dissolved	Altered	Residual	Sum	Quartz	Feldspar	Clay	Other	Sum
P1	Peridotite	0.395	0.164	0.443	1	0.000	0.076	0.186	0.738	1
P2	Gabbro	0.181	0.417	0.402	1	0.000	0.289	0.492	0.219	1
P3	Diorite	0.195	0.411	0.393	1	0.000	0.290	0.492	0.218	1
P4	Granodiorite	0.043	0.025	0.930	1	0.259	0.638	0.026	0.077	1
P5	Granite	0.027	0.023	0.951	1	0.360	0.541	0.024	0.076	1
P6	Anorthosite	0.077	0.057	0.867	1	0.000	0.890	0.057	0.053	1
P7	Syenite	0.036	0.027	0.936	1	0.052	0.824	0.028	0.096	1
V1	Basalt	0.163	0.064	0.773	1	0.000	0.483	0.063	0.454	1
V2	Andesite	0.047	0.038	0.915	1	0.149	0.443	0.040	0.368	1
V3	Rhyolite	0.037	0.026	0.935	1	0.229	0.446	0.027	0.298	1
S1	Q sandstone	0.012	0.003	0.985	1	0.885	0.086	0.003	0.025	1
S2	Arkose	0.060	0.015	0.926	1	0.505	0.377	0.016	0.102	1
S3	Greywacke	0.108	0.014	0.877	1	0.505	0.265	0.016	0.214	1
S4	Mudstone	0.049	0.006	0.945	1	0.315	0.040	0.639	0.005	1
S5	Carbonate	0.751	0.001	0.248	1	0.602	0.113	0.205	0.080	1
M1	Metasandstone	0.008	0.011	0.981	1	0.554	0.288	0.011	0.147	1
M2	Slate	0.034	0.005	0.960	1	0.311	0.039	0.629	0.021	1
M3	Marble	0.751	0.001	0.248	1	0.602	0.113	0.205	0.080	1
M4	Schist/phyllite	0.014	0.027	0.960	1	0.051	0.097	0.027	0.826	1
M5	Gneiss, plag	0.013	0.015	0.974	1	0.253	0.481	0.015	0.251	1
M6	Gneiss, Kspar	0.011	0.018	0.972	1	0.253	0.483	0.018	0.246	1

Table 14 – Summary Results for All PL under Intermediate Weathering

PL	Short Name	Dissolved	Altered	Residual	Sum	Quartz	Feldspar	Clay	Other	Sum
P1	Peridotite	0.643	0.263	0.095	1	0.000	0.000	0.474	0.526	1
P2	Gabbro	0.272	0.671	0.057	1	0.000	0.000	0.886	0.114	1
P3	Diorite	0.290	0.663	0.046	1	0.000	0.000	0.895	0.105	1
P4	Granodiorite	0.135	0.146	0.716	1	0.286	0.527	0.170	0.017	1
P5	Granite	0.104	0.137	0.759	1	0.391	0.432	0.153	0.024	1
P6	Anorthosite	0.293	0.331	0.376	1	0.000	0.508	0.459	0.033	1
P7	Syenite	0.082	0.108	0.810	1	0.054	0.792	0.117	0.037	1
V1	Basalt	0.400	0.219	0.380	1	0.000	0.568	0.333	0.099	1
V2	Andesite	0.306	0.255	0.439	1	0.205	0.402	0.368	0.026	1
V3	Rhyolite	0.255	0.160	0.584	1	0.296	0.483	0.215	0.006	1
S1	Q sandstone	0.022	0.018	0.961	1	0.894	0.072	0.019	0.016	1
S2	Arkose	0.104	0.086	0.811	1	0.530	0.309	0.096	0.065	1
S3	Greywacke	0.152	0.097	0.751	1	0.531	0.217	0.114	0.138	1
S4	Mudstone	0.059	0.021	0.921	1	0.319	0.037	0.639	0.005	1
S5	Carbonate	0.754	0.005	0.240	1	0.610	0.083	0.225	0.081	1
M1	Metasandstone	0.037	0.058	0.905	1	0.571	0.256	0.060	0.113	1
M2	Slate	0.046	0.020	0.934	1	0.314	0.033	0.632	0.021	1
M3	Marble	0.754	0.005	0.240	1	0.610	0.083	0.225	0.081	1
M4	Schist/phyllite	0.095	0.213	0.692	1	0.055	0.091	0.235	0.619	1
M5	Gneiss, plag	0.053	0.060	0.888	1	0.264	0.420	0.063	0.253	1
M6	Gneiss, Kspar	0.042	0.074	0.885	1	0.261	0.456	0.077	0.206	1

Table 15 – Summary Results for All PL under Advanced Weathering

PL	Short Name	Dissolved	Altered	Residual	Sum	Quartz	Feldspar	Clay	Other	Sum
P1	Peridotite	0.670	0.271	0.060	1	0.000	0.000	0.537	0.463	1
P2	Gabbro	0.292	0.677	0.031	1	0.000	0.000	0.920	0.080	1
P3	Diorite	0.310	0.668	0.021	1	0.000	0.000	0.928	0.072	1
P4	Granodiorite	0.297	0.341	0.360	1	0.352	0.160	0.487	0.001	1
P5	Granite	0.239	0.305	0.456	1	0.460	0.126	0.401	0.013	1
P6	Anorthosite	0.427	0.511	0.062	1	0.000	0.091	0.880	0.029	1
P7	Syenite	0.256	0.376	0.368	1	0.067	0.400	0.506	0.027	1
V1	Basalt	0.527	0.358	0.115	1	0.000	0.196	0.715	0.089	1
V2	Andesite	0.421	0.384	0.195	1	0.245	0.092	0.663	0.000	1
V3	Rhyolite	0.363	0.301	0.335	1	0.346	0.181	0.473	0.000	1
S1	Q sandstone	0.043	0.047	0.911	1	0.914	0.024	0.049	0.014	1
S2	Arkose	0.184	0.199	0.618	1	0.582	0.113	0.244	0.061	1
S3	Greywacke	0.208	0.180	0.612	1	0.568	0.078	0.227	0.126	1
S4	Mudstone	0.148	0.163	0.688	1	0.352	0.016	0.626	0.006	1
S5	Carbonate	0.761	0.014	0.226	1	0.627	0.024	0.266	0.084	1
M1	Metasandstone	0.115	0.159	0.727	1	0.621	0.087	0.179	0.113	1
M2	Slate	0.139	0.147	0.714	1	0.348	0.008	0.620	0.023	1
M3	Marble	0.761	0.014	0.226	1	0.627	0.024	0.266	0.084	1
M4	Schist/phyllite	0.193	0.348	0.458	1	0.062	0.032	0.432	0.475	1
M5	Gneiss, plag	0.206	0.237	0.557	1	0.315	0.130	0.299	0.256	1
M6	Gneiss, Kspar	0.153	0.244	0.603	1	0.295	0.213	0.289	0.204	1

Table 16 – Summary Results for All PL under Extreme Weathering

PL	Short Name	Dissolved	Altered	Residual	Sum	Quartz	Feldspar	Clay	Other	Sum
P1	Peridotite	0.670	0.271	0.060	1	0.000	0.000	0.537	0.463	1
P2	Gabbro	0.292	0.677	0.031	1	0.000	0.000	0.920	0.080	1
P3	Diorite	0.310	0.668	0.021	1	0.000	0.000	0.928	0.072	1
P4	Granodiorite	0.342	0.408	0.248	1	0.377	0.000	0.622	0.002	1
P5	Granite	0.278	0.362	0.360	1	0.485	0.000	0.501	0.014	1
P6	Anorthosite	0.449	0.541	0.010	1	0.000	0.000	0.969	0.031	1
P7	Syenite	0.367	0.563	0.070	1	0.079	0.000	0.889	0.032	1
V1	Basalt	0.565	0.413	0.022	1	0.000	0.000	0.904	0.096	1
V2	Andesite	0.444	0.414	0.142	1	0.255	0.000	0.745	0.000	1
V3	Rhyolite	0.407	0.372	0.220	1	0.372	0.000	0.628	0.000	1
S1	Q sandstone	0.052	0.061	0.888	1	0.922	0.000	0.064	0.014	1
S2	Arkose	0.220	0.256	0.525	1	0.608	0.000	0.328	0.064	1
S3	Greywacke	0.232	0.218	0.550	1	0.586	0.000	0.284	0.130	1
S4	Mudstone	0.272	0.362	0.366	1	0.412	0.000	0.581	0.007	1
S5	Carbonate	0.763	0.017	0.220	1	0.633	0.000	0.283	0.084	1
M1	Metasandstone	0.145	0.205	0.650	1	0.643	0.000	0.240	0.117	1
M2	Slate	0.262	0.318	0.420	1	0.406	0.000	0.566	0.027	1
M3	Marble	0.763	0.017	0.220	1	0.633	0.000	0.283	0.084	1
M4	Schist/phyllite	0.290	0.460	0.250	1	0.070	0.000	0.648	0.282	1
M5	Gneiss, plag	0.274	0.327	0.400	1	0.344	0.000	0.450	0.206	1
M6	Gneiss, Kspar	0.231	0.369	0.400	1	0.325	0.000	0.480	0.195	1

4 PRACTICAL APPLICATION

4.1 Permo-Triassic Boundary, Bavaria

The Permo-Triassic boundary section to the southwest of the Bohemian Massif in Bavaria, as documented in boreholes Lindau-1 and Obernsees-1 (Figure 3), has been the subject of geological investigations to: document the sedimentological evolution of the strata (Ravidà et al. 2021a); to unravel the rate at which the sediments were delivered (Ravidà et al. 2021b); and to discern the provenance of the sediment (Caracciolo et al., 2021). All these kinds of investigations would be more precise if there were a quantitative expectation for the relative contribution of different lithologies eroded from the landscape to the sediment supply, similar to the Sand Generation Index of Palomares and Arribas (1993), but also including clays.

The cited body of work about the Bohemian Permo-Triassic, and the previous decades of geologic investigation on which it is based, demonstrate that the climate became wetter from the Permian to the Triassic, which had the effect of flushing more sediment off the landscape. However, the wetter climate also probably had the effect of increasing the fraction of landscape dissolved during denudation compared to the drier climate. There were also variations in the relative abundance of plutonic, low-grade metamorphic, and high-grade metamorphic rocks contributing to the sediment supply over time. It is certain that the dissolution of granitic, low-grade metamorphic, and high-grade metamorphic rocks did not respond in exactly same way to the increasing weathering intensity of the wetter climate: removing 10 m of each type of provenance-lithotype assemblage from 1 km2 of landscape would erode 0.1 km3 of rock, but each type would not contribute the same amount, nor the same kind, of sediment to the transport system.

The DARE approach offers a pathway to quantitatively estimate the relative contribution of each PL-assemblage under each set of weathering conditions, and to set an expectation for the gross mineralogy of each contribution. This level of constraint permits more rigorous evaluation of the relative influence of climate and provenance lithology in determining the characteristics of deposited sediments.

The example calculations below merely illustrate how the method can be applied to a subset of the hinterland geology of the Franconian Basin in Bavaria using the generalized PL descriptions provided in this paper. It is certainly possible to make a more refined analysis using customized PL descriptions tailored to specific geological formations, and to broaden the analysis to a wider spectrum of geology.

Figure 2 – Location of Boreholes Lindau-1 and Obernsees-1, which document the Permo-Triassic boundary in Bavaria

4.2 Bavarian Geologic Setting

4.2.1 The Hercynia River

The wells Lindau-1 and Obernsees-1 record fluvial deposits of a river that flowed from present-day SW to NE along a structurally defined corridor parallel to the Pfahl, Danube, and Franconian faults, with headwaters near the present-day Bavarian-Austrian border; Ravidà et al. 2021b and Caracciolo et al. 2021 dub this the Hercynia river (Figure 4).

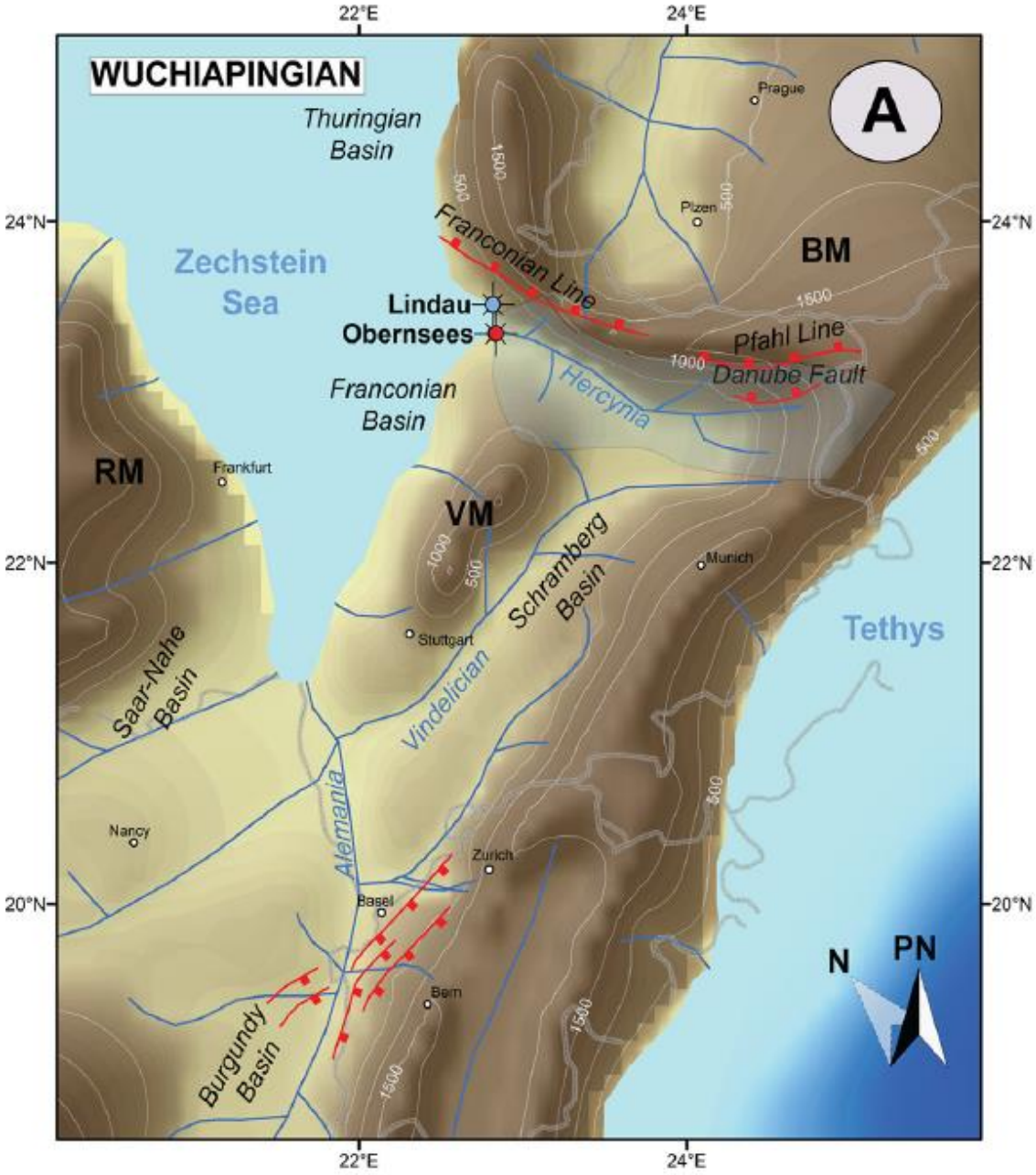

Figure 3 – Location of wells Lindau-1 and Obernsess-1 along the paleo-Hercynia River during the late Permian (after Ravidà et al. 2021b, Fig 4; paleogeography from Getech Group plc). PN = PaleoNorth; paleoelevation contours in meters; present day political boundaries rotated to paleoposition for reference.

4.2.2 Hinterland Geology

As documented by Ravidà et al. 2021a and evaluated by Caracciolo et al. 2021 (Figure 5), both metamorphic rocks of the Moldanubian Terrane, as well as Variscan granites, contributed to the sediments at Lindau and Obersees at different times.

Typical examples of both Moldanubian high-grade metamorphics and late Variscan granites are exposed today around the village of Hauzenberg, Bavaria (south of the “l” in Pfahl in Figure 5). These rocks are represented on the 1:25 000 digital geological map 7347 Hauzenberg, published by the Bayerischen Landesamt für Umwelt (https://www.lfu.bayern.de/download/geologie/dgk25/dGK25_7347_hauzenberg.pdf). Table 17 and Table 18 report the relative areal abundance of various map units from the 7347 Hauzenberg map and assign each map unit to a provenance lithotype from Table 1. Table 1 is not intended to definitively characterize any portion of the Permo-Triassic landscape of Franconia; rather it provides a modern analogue that might approximate two of the end-member geologic assemblages present on that landscape.

It should be noted that Heins & Kairo 2007 did not include amphibolite (Amfibolit in Table 18) or meta-ultramafics (Meta-Ultramafitit of Table 18) among their PL. Here we assume amphibolite to be composed primarily of amphibole and plagioclase (either calcic or sodic), which means it should be similar to either gabbro or diorite, so we consider half of the mapped amphibolite to be gabbro (P1 in Table 1) and half to be diorite (P3 in Table 1). In the same way, we treat meta-ultramafite as mineralogically equivalent to peridotite (P1 in Table 1).

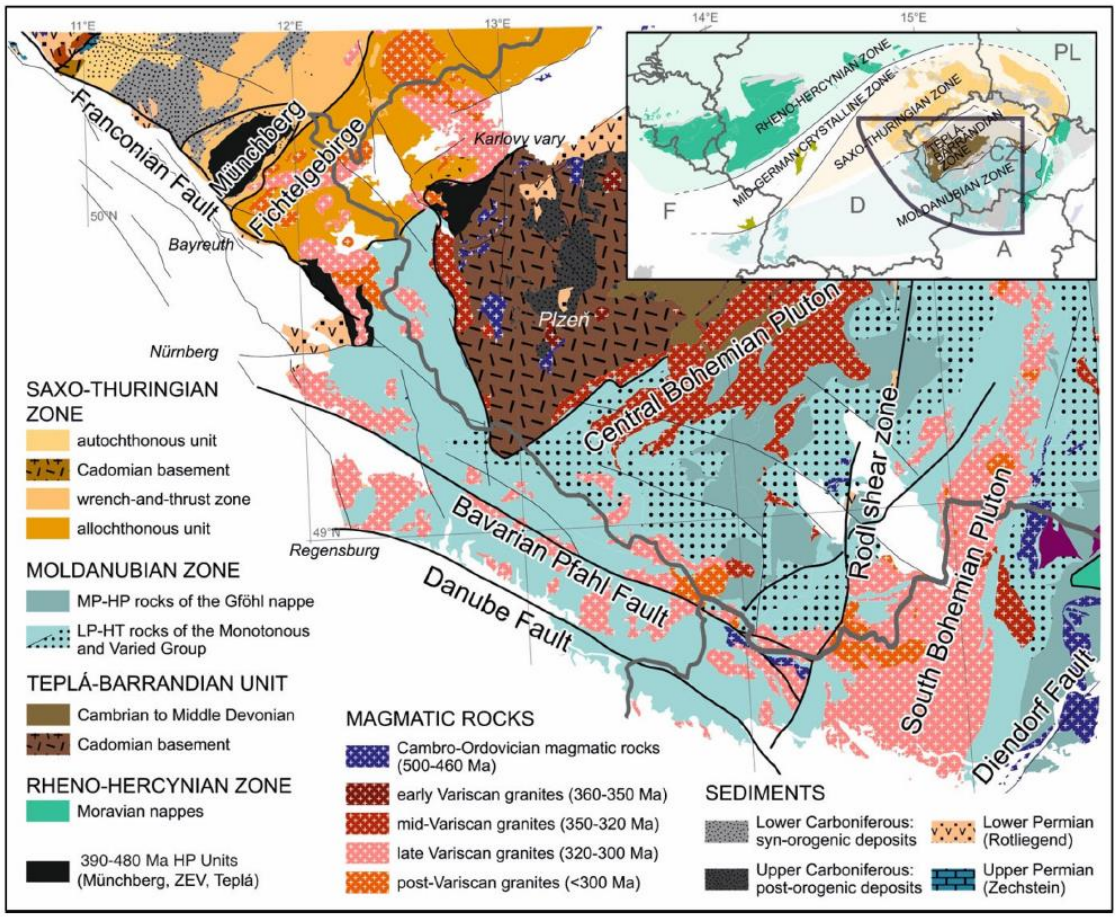

Figure 4 – Geology of the Bohemian Massif along the Bavarian-Czech Border(after Caracciolo et al. 2021, Fig. 2)

Table 17– Geological Units and Provenance Lithotypes of the Hauzenberger Pluton (HZ) and Moldanubium (MO) near Hauzenberg, Bavaria

Map Symbol	Unit Name	PL	Fraction (area/area)
HZ,Gg	Gangesteine	V3	0.01
HZ, GDr	Biotit-Granodiorit, fein- bis mittlekörnig	P4	0.24
HZ, Grf	Biotit-Muskovit-Granit, feinkörnig	P5	0.25
HZ, Grm	Biotit-Muskovit-Granit, mittlekörnig	P5	0.50
Sum			1
MO,Am	Amfibolit	P2	0.04
MO,Am	Amfibolit	P3	0.04
MO,bpGn$_{mx}$,ba	Metatektisher Biotit-Plagioklas-Gneis	M5	0.80
MO,KS	Kalksilikatgestein	M3	0.03
MO,lkGn	Leukokrater Gneis	M6	0.06
MO,mMPu	Meta-Ultramafitit	P1	0.03
Sum			1

4.3 Bavarian Application of DARE

The environmental conditions documented by Ravidà et al. 2021b range from hot and arid (Mean Annual Temperature 40°C, Mean Annual Runoff 40 mm/yr) in the mid Permian (Roadian) to cooler and wetter (33.5°C, 183 mm/yr) in the early Triassic (Induan). Using the logic of Heins & Kairo 2007, we might expect the weathering intensity in the sense of DARE to be somewhere between Incipient to Intermediate. Weighting the expected outcomes of Table 13 (Incipient) and Table 14 (Intermediate) by the expected PL abundance for the Variscan granite PL assemblage, and the Moldanubian metamorphic assemblage, we can derive an expectation for the relative magnitude of dissolution, and for the relative abundance of different minerals, across the different combinations of PL assemblage and weathering intensity (Table 19, visualized in Figure 6). Although these results are reported to 3 significant figures, they should be treated as qualitative results. Nevertheless, these qualitative results highlight subtle but important differences between provenance lithotype assemblages and weathering conditions that would not have been apparent without this systematic and quantitative analysis.

96 **Table 18 – Summary DARE output (v/v fractions) for alternate hinterland geology**

	Incipient Weathering	Intermediate Weathering
Granitic Hinterland (Hauzenberger Pluton)		
Dissolved	0.031	0.113
Altered	0.024	0.139
Residual	0.945	0.747
Sum	**1**	**1**
Quartz	0.334	0.365
Feldspar	0.563	0.455
Clay	0.024	0.157
Other	0.078	0.022
Sum	**1**	**1**
F:Q	1.69	1.25
Metamorphic Hinterland (Hauzenberger Moldanubicum)		
Dissolved	0.060	0.109
Altered	0.051	0.114
Residual	0.890	0.778
Sum	**1**	**1**
Quartz	0.236	0.245
Feldspar	0.442	0.366
Clay	0.064	0.147
Other	0.258	0.242
Sum	**1**	**1**
F:Q	1.88	1.49

97

98

99

Figure 5 – Comparison of Expected Weathering Volumes and Products

4.4 Evaluation of Bavarian Results

Changes in the volume and character of sediment delivered by the Hercynia River to the deposits at Lindau and Obernsees represent the integrated effect of changes in hinterland geology, climate, and tectonics. The integrated effect has multiple causes that must be evaluated holistically to derive proper conclusions: it is wrong to say there is a "climate signal" or a "geology signal" or a "tectonic signal". For example, a stratigraphic change from more to less feldspathic sand could be attributed either to increased weathering (intensity, due to climate ± duration, due to regional topographic gradient), or to a more granitic hinterland. If climate, topography, and exposed geology change at the same time, the effect of one may be enhanced or attenuated by the effect of the other. From the DARE results, at lower weathering, the dissolved fraction of the metamorphic assemblage is nearly twice as great as that for the granitic assemblage, whereas at higher weathering the granitic dissolved fraction is slightly more than the metamorphic one. For both assemblages the dissolved fraction increases with increasing weathering intensity, so that even though more sediment is produced at higher weathering intensity, it takes relatively more provenance lithotype to yield a fixed amount of sediment. The qualitative results of the DARE model highlight subtle but important differences between provenance lithotype assemblages and weathering conditions that would not have been apparent without this systematic and quantitative analysis.

5 DISCUSSION AND CONCLUSIONS

DARE is intended to address the approximate magnitude of the gross discrepancy between the volume of sediment produced on the hinterland and the volume deposited in the basin, over long time and length scales, to make mass-balance calculations more accurate so that multiple sources for a single widespread stratigraphic unit, or bypass of the unit, might be more easily detected (Heins 2023). DARE integrates modifications to the sediments over an entire Sediment Routing System (Allen 2008, Allen 2017) from the erosional engine, through the transfer zone, and into the long-term sink. DARE is not intended to help decipher in detail the myriad tectonic, climatic, and geomorphic perturbations that can befall the system, and which may or may not be clearly recorded in the stratigraphic record (Castelltort & Van Den Driessche 2003, Allen 2008, Romans et al. 2016, Toby et al. 2019). The challenges involved for full understanding of the entire Sediment Routing System and for a full Quantitative Provenance Analysis (Weltje and von Eynatten 2004) are well enumerated by Weltje 2012 and Caracciolo 2020; DARE is not for that purpose.

In the Bavarian example, DARE can illustrate that tectonics (in the construction of the PL assemblage) AND climate (in the intensity of weathering) AND geomorphology (in the duration and trajectory of transport) will all play a role in the original roster and ultimate modification of the minerals on the landscape. DARE can start the fundamental differentiation between the role of PL mineralogy and the integrated effect of weathering intensity and duration, but it cannot unravel the relative contribution of weathering intensity and duration, nor elucidate fine-scale stratigraphic or geographic mineralogic differences that arise from variable connectivity of different landscape elements.

DARE puts rough geochemical boundaries around the mineralogical changes that can occur across the spectrum from no alteration of a PL to the maximal alteration possible. In this sense, it might be applied to help investigate the relative ability of different PL to:

- generate dissolved ions (Allen & Allen 2013, Chapter 7.2.2);
- supply specific minerals ("mineral fertility" -- Moecher & Samson 2006, Malusà et al. 2013, Flowerdew et al. 2019, Garzanti & Andò, 2019; Chew et al. 2020); or
- supply specific size fractions (especially sand, "Sand Generation Index" – Palomares & Arribas 1993, Le Pera et al. 2001, Arribas & Tortosa 2003, Garzanti 2019).

Acknowledgments

Early versions of this manuscript benefited greatly from comments by Luca Caracciolo and Melise Harland and discussions with Meg Galsworthy and Laura Tierney.

References

Allen PA, 2008, From landscapes into geological history: Nature, v. 451, p. 274-276. https://doi.org/10.1038/nature06586

Allen PA, 2017, Sediment Routing Systems The Fate of Sediment from Source to Sink: Cambridge University Press. 407 p. https://doi.org/10.1017/9781316135754

Allen PA, Allen JR, 2013, Basin Analysis: Principles and Application to Petroleum Play Assessment, 3rd Edition: Wiley-Blackwell, ISBN 978-0-470-67377-5.

Allen PA, Armitage JJ, Carter A, Duller RA, Michael NA, Sinclair HD, Whitchurch AL, Whittaker AC, 2013, The Qs problem: sediment volumetric balance of proximal foreland basin systems: Sedimentology v. 60, p. 102–130. https://doi.org/10.1111/sed.12015

Arribas J, Tortosa A, 2003, Detrital modes in sedimenticlastic sands from low-order streams in the Iberian Range, Spain: the potential for sand generation by different sedimentary rocks: Sedimentary Geology, v. 159, p. 275-303. https://doi.org/10.1016/S0037-0738(02)00332-9

Armitage JJ, Duller RA, Whittaker AC, Allen PA, 2011, Transformation of tectonic and climatic signals from source to sedimentary archive: Nature Geoscience, v. 4, p. 231–235. https://doi.org/10.1038/ngeo1087

Armitage JJ, Dunkley Jones, T, Duller RA, Whittaker AC, Allen PA, 2013, Temporal buffering of climate-driven sediment flux cycles by transient catchment response: Earth and Planetary Science Letters, v. 369, p. 200–210. https://doi.org/10.1016/j.epsl.2013.03.020

Barnes JB, Heins, WA, 2009, Plio-Quaterary mass balance between thrust belt erosion and foreland deposition in the central Andes, southern Bolivia: Basin Research, v. 21, p. 91-109, https://doi.org/10.1111/j.1365-2117.2008.00372.x

179 Börker J, Hartmann J, Amann T, Romero-Muhalli G, 2018, Terrestrial sediments of the Earth:
180 Development of a Global Unconsolidated Sediments map database (GUM): Geochemistry,
181 Geophysics, Geosystems, v 19, p 997-1024, https://doi.org/10.1002/2017GC007273

182 Brengman LA, Heins WA, Matthews JA, 2016, Dissolution and transformation of provenance
183 lithotypes during initial sediment generation with application to play-element prediction:
184 ExxonMobil Upstream Research Company Research Application Report URC.2016.046

185 Brantley, S.L., 2008. Kinetics of Mineral Dissolution, in Kinetics of water-rock interaction,
186 Brantley, S.L., Kubicki, J.D., White, A.F. (eds): Berkeley, University of California Press,
187 Chapter 5. e-ISBN 978-0-387-73563-1

188 Caracciolo L, 2020, Sediment generation and sediment routing systems from a quantitative
189 provenance analysis perspective: review, application and future development: Earth-
190 Science Reviews, v. 209, 103226. https://doi.org/10.1016/j.earscirev.2020.103226

191 Caracciolo L, Ravidà DCG, Chew D, Janßen M, Lünsdorf, NK, Heins WA, Stephan T,
192 Stollhofen H, 2021, Reconstructing environmental signals across the Permian-Triassic
193 boundary in the SE Germanic Basin: A Quantitative Provenance Analysis (QPA) approach:
194 Global and Planetary Change, v 206, 103631,
195 https://doi.org/10.1016/j.gloplacha.2021.103631

196 Castelltort S, Van Den Driessche J, 2003, How plausible are high-frequency sediment supply-
197 driven cycles in the stratigraphic record?: Sedimentary Geology, v. 157, p. 3–13.
198 https://doi.org/10.1016/S0037-0738(03)00066-6

199 Chew D, O'Sullivan G, Caracciolo L, Mark C, Tyrrell S, 2020, Sourcing the sand: accessory
200 mineral fertility, analytical and other biases in detrital U-Pb provenance analysis: Earth-
201 Science Reviews, v. 202, 103093, https://doi.org/10.1016/j.earscirev.2020.103093

202 Clark, K.F., 1982, Mineral composition of rocks, in Carmichael, R.S., ed.,Handbook of Physical
203 Properties of Rocks, Volume 1: Boca Raton, CRC Press, p. 1–213.

204 Crovisier, J.L., Honnorez, J., Eberhart, J. P., 1987. Dissolution of basaltic glass in seawater:
205 Mechanism and rate. Geochimica et Cosmochimica Acta. Vol. 51, p. 2977-2990.
206 https://doi.org/10.1016/0016-7037(87)90371-1

207 DePalma A, 2008, Bluestone boom opens quarries to new allies, and to change: New York
208 Times, 13 May 2008, https://www.nytimes.com/2008/05/13/nyregion/13quarry.html
209 (visited 25 Jul 2023).

210 Dürr HH, Meybeck M, Dürr SH, 2005, Lithologic composition of the Earth's continental
211 surfaces derived from a new digital map emphasizing riverine material transfer: Global
212 Biogeochemical Cycles, v. 19, GB4S10 https://doi.org/10.1029/2005GB002515

213 Ebner D, 2006, Chevron risks the deep: The Globe and Mail, 30 July 2006,
214 https://www.theglobeandmail.com/report-on-business/chevron-risks-the-
215 deep/article20412515/ (visited 25 Jul 2023)

216 Fischer C, Luttge A, 2017, Beyond the conventional understanding of water-rock reactivity:
217 Earth and Planetary Science Letters, v. 457, p. 100-105.
218 https://doi.org/10.1016/j.epsl.2016.10.019

Flowerdew MJ, Fleming EJ, Morton AC, Frei D, Chew DM, Daly JS, 2019, Assessing mineral fertility and bias in sedimentary provenance studies: examples from the Barents Shelf: Geological Society, London, Special Publication 484, p. 255-274. https://doi.org/10.1144/SP484.11

Garzanti E, 2019, Petrographic classification of sand and sandstone: Earth-Science Reviews, v. 192, p. 545-563. https://doi.org/10.1016/j.earscirev.2018.12.014

Garzanti E, Andò S, 2019, Heavy mineral for junior woodchucks: Minerals, v. 9, 148, https://doi.org/10.3390/min9030148

Garzanti E, Resentini A, 2016, Provenance control on chemical indices of weathering (Taiwan river sands): Sedimentary Geology, v. 336, p. 81-95. https://doi.org/10.1016/j.sedgeo.2015.06.013

Hartmann J, Moosdorf N, 2012, The new global lithological map database GLiM: a representation of rock properties at the Earth surface: Geochemistry, Geophysics, Geosystems, v13, Q12004, https://doi.org/10.1029/2012GC004370 .

Hatzenbühler D, Caracciolo L, Weltje GJ, Praquive A, Regelous M,2022, Lithologic, geomorphic, and climatic controls on sand generation from volcanic rocks in the Sierra Nevada de Santa Marta massif (NE Colombia): Sedimentary Geology, v. 429, 106076. https://doi.org/10.1016/j.sedgeo.2021.106076

Heins WA, 1993, Source-rock texture vs. climate and topography as controls on the composition of modern, plutoniclastic sand: Geological Society of America Special Paper 284, p. 135-146. https://doi.org/10.1130/SPE284-p135

Heins WA, 2023, Honest bookkeeping for source-to-sink sediment mass-balance analysis with examples from the Angoche Margin of Mozambique and the Corsica Trough of France: Journal of Marine and Petroleum Geology, v. 153, 106265. https://doi.org/10.1016/j.marpetgeo.2023.106265

Heins WA, Bailey CH, 2020, Estimating spatially and temporally relevant denudation rates for sediment mass balance studies of hydrocarbon reservoirs: ResTech Virtual Reservoir Conference, European Association of Geoscientists and Engineers, 22 Apr 2020, https://doi.org/10.3997/2214-4609.202RESTECH07

Heins WA, Kairo S, 2007, Predicting sand character with integrated genetic analysis: Geological Society of America Special Paper 420 p 345-379. https://doi.org/10.1130/2006.2420(20)

Jin LX, Ravella R, Ketchum B, Bierman PR, Heaney P, White T, Brantley SL, 2010, Mineral weathering and elemental transport during hillslope evolution at the Susquehanna/Shale Hills Critical Zone Observatory: Geochimica et Cosmochimica Acta, v. 74, p. 3669-3691. https://doi.org/10.1016/j.gca.2010.03.036

Kairo S, Heins WA, Love KM, 2010, Predicting Sand-Grain Composition and Texture, United States Patent 7,747,552 B2, issued 29 June, 2010

Kirkman, J.,H., McHardy, W.J., 1980. A comparative study of the morphology, chemical composition and weathering of rhyolitic and andesitic glass. Clay Minerals, 15, 165-173. https://doi.org/10.1180/claymin.1980.015.2.07

Lasaga AC, Soler JM, Ganor J, Burch TE, Nagy KL, 1994, Chemical weathering rate laws and global geochemical cycles: Geochimica et Cosmochimica Acta, v58 p2361-2386. https://doi.org/10.1016/0016-7037(94)90016-7

Le Pera E, Arribas J, Critelli S, Tortosa A, 2001, The effects of source rocks and chemical weathering on the petrogenesis of siliciclastic sand from the Neto river (Calabria, Italy): implications for provenance studies: Sedimentology, v. 48, p. 357-378. https://doi.org/10.1046/j.1365-3091.2001.00368.x

Malusà MG, Carter A, Limoncelli M, Villa IM, Garzanti E, 2013, Bias in detrital zircon geochronology and thermochronometry: Chemical Geology, v. 359, p. 90-107. https://doi.org/10.1016/j.chemgeo.2013.09.016

Markwick PJ, Valdes PJ, 2004, Palaeo-digital elevation models for use as boundary conditions in coupled ocean–atmosphere GCM experiments: a Maastrichtian (late Cretaceous) example: Palaeogeography, Palaeoclimatology, Palaeoecology, v. 213, p. 37–63, https://doi.org/10.1016/j.palaeo.2004.06.015

Meister R, Robertson EC, Werre RW, Raspet R, 1980, Elastic Moduli of Rock Glasses Under pressure to 8 kBar and geophysical implications: Journal of Geophysical Research, v85 nB11 p6461-6470. https://doi.org/10.1029/JB085iB11p06461

Moecher DP, Samson SD, 2006, Differential zircon fertility of source terranes and natural bias in the detrital zircon record: implications for sedimentary provenance analysis: Earth and Planetary Science Letters, v. 247, p. 252-266. https://doi.org/10.1016/j.epsl.2006.04.035

Nesbitt, H.W., Markovics, G., 1997. Weathering of granodioritic crust, long-term storage of elements in weathering profiles and petrogenesis of siliciclastic sediments. Geochimica et Cosmochimica Acta, v. 61, no. 8, pp. 1653-1670. https://doi.org/10.1016/S0016-7037(97)00031-8

Nesbitt, H.W., Wilson, R.E., 1992. Recent chemical weathering of basalts. American Journal of Science, v. 292, p. 740-777. https://doi.org/10.2475/ajs.292.10.740

Nesbitt HW, Young GM, 1982, Early Proterozoic climates and plate motions inferred from major element chemistry of lutites: Nature, v. 299, p. 715-717. https://doi.org/10.1038/299715a0

Nesbitt HW, Young GM, McLennan SM, Keays RR, 1996, Effects of chemical weathering and sorting on the petrogenesis of siliciclastic sediments, with implications for provenance studies: Journal of Geology, v 104, p525-542. https://doi.org/10.1086/629850

Palomares M, Arribas J, 1993, Modern stream sands from compound crystalline sources: composition and sand generation index: Geological Society of America Special Paper 284, p. 313-322. https://doi.org/10.1130/SPE284-p313

Phillips WR & Griffen DT, 1981, Optical Mineralogy The Nonopaque Minerals: WH Freeman.

Poręba G, Śnieszko, Moska P, Mroczek P, Malik I, 2019, Interpretation of soil erosion in a Polish loess area using OSL, 137Cs, 210Pbex, dendrochronology and micromorphology – case study: Biedrzykowice site (S Poland): Geochronometria, v. 46, p. 57-78, https://doi.org/10.1515/geochr-2015-0109

Railsback LB, 2007, Goldich's Weathering Series explained in terms of bond strength: Some Fundamentals of Mineralogy and Geochemistry, http://railsback.org/Fundamentals/8150Goldich&BondStreng06LS.pdf

Ravidà DCG, Caracciolo L, Henares S, Janßen M, Stollhofen H, 2021a, Drainage and environmental evolution across the Permo–Triassic boundary in the south-east Germanic Basin (north-east Bavaria): Sedimentology, v69, p501-536. https://doi.org/10.1111/sed.12913

Ravidà DCG, Caracciolo L, Heins WA, Stollhofen H, 2021b, Reconstructing environmental signals across the Permian-Triassic boundary in the SE Germanic Basin: paleodrainage modelling and quantification of sediment flux: Global and Planetary Change, v206 n103632 https://doi.org/10.1016/j.gloplacha.2021.103632

Ravidà DCG, Caracciolo L, Heins WA, Stollhofen H, 2023, Towards improved discrimination and correlation of Permian-Early Triassic sediments in Central Europe: a chemostratigraphic approach: Sedimentary Geology, v 452, 106408, https://doi.org/10.1016/j.sedgeo.2023.106408

Romans BW, Castelltort S, Covault JA, Fildani A, Walsh JP, 2016, Environmental signal propagation in sedimentary systems across time scales: Earth-Science Reviews, v. 153, p. 7-29. https://doi.org/10.1016/j.earscirev.2015.07.012

Sadler PM, Jerolmack DJ, 2014, Scaling laws for aggradation, denudation and progradation rates: the case for time-scale invariance at sediment sources and sinks: Geological Society, London, Special Publication 404, Chapter 7. https://doi.org/10.1144/SP404.7

Schroeder, P.A., Melear, N.D., West, L.T., Hamilton, D.A., 2000. Meta-gabbro weathering in the Georgia Peidmont, USA: implications for globala silicate weathering rates. Chemical Geology, 163, 235-245. https://doi.org/10.1016/S0009-2541(99)00129-1

Stewart RJ, Hallet B, Zeitlar PK, Malloy MA, Allen CM, Trippett D, 2008, Brahmaputra sediment flux dominated by a highly localized rapid erosion from the easternmost Himalaya: Geology, v. 36, p. 711-714. https://doi.org/10.1130/G24890A.1

Stoch L, Sikora W, 1976, Transformation of micas in the process of kaolinitization of granites and gneisses: Clays and Clay Minerals, v. 24, p. 156-162.

Taylor TR, Lander RH, Bonnell LM, 2022. Modeling sandstone diagenesis and rock properties: Society of Economic Paleontologists and Mineralogists Concepts in Sedimentology and Paleontology 13, Chapter 12. https://doi.org/10.2110/sepmcsp.13.12

Toby SC, Duler RA, De Angelis S, Straub KM, 2019, A stratigraphic framework for the preservation and shredding of environmental signals: Geophysical Research Letters, v. 46, p. 5837-5845. https://doi.org/10.1029/2019GL082555

van der Weijden CH, Pacheco FAL, 2003, Hydrochemistry, weathering and weathering rates on Madeira Island: Journal of Hydrology, v. 283, p. 122-145. https://doi.org/10.1016/S0022-1694(03)00245-2

Velbel MA, 1984, Weathering Processes of Rock-Forming Minerals: Environmental Chemistry, Mineralogical Association of Canada Short Course Handbook, v. 10, p. 67-111.

339 Weltje GJ, 2012, Quantitative models of sediment generation and provenance: State of the art
340 and future developments: Sedimentary Geology, v. 280, p. 4-20.
341 https://doi.org/10.1016/j.sedgeo.2012.03.010

342 Weltje GJ, von Eynatten H, 2004 Quantitative provenance analysis of sediments: review and
343 outlook: Sedimentary Geology, v. 171, p. 1-11.
344 https://doi.org/10.1016/j.sedgeo.2004.05.007

345 Weltje GJ, Meijer XD, De Boer PL, 1998, Stratigraphic inversion of siliciclastic basin fills: a
346 note on the distinction between supply signals resulting from tectonic and climatic forcing:
347 Basin Research, v. 10, p. 129-153. https://doi.org/10.1046/j.1365-2117.1998.00057.x

348 Wohletz K, Heiken G, 1992, Volcanology and Geothermal Energy: Berkeley, University of
349 California Press: http://ark.cdlib.org/ark:/13030/ft6v19p151/ , Appendix B, Table B.5

350 Wolff-Boenish D, Gislason SR, Oelkers EH, Putins CV, 2004, The dissolution rates of natural
351 glasses as a function of their composition at pH4 and 10.6, and temperatures from 25 to
352 74°C: Geochimica et Cosmochimica Acta, v. 68, p. 4843-4858.
353 https://doi.org/10.1016/j.gca.2004.05.027

354 Yuan GH, Cao YC, Schultz HM, Hao F, Gluyas J, Liu KY, Yang T, Wang YZ, Xi KL, Li FL,
355 2019, A review of felspar alteration and its geological significance in sedimentary basins:
356 From shallow aquifers to deep hydrocarbon reservoirs: Earth-Science Reviews v191 p114-
357 140 Equation 25. https://www.sciencedirect.com/science/article/pii/S0012825217305512
358 .

A mineralogic approach to estimating the volume of dissolution, alteration, and unaltered residue from weathering of different provenance lithotypes

William A. Heins[1], Lathisha A. Brengman[2]

[1]Getech Group plc..

[2]Department of Earth and Environmental Science, University of Minnesota-Duluth.

Corresponding author: William A Heins (bill.heins@getech)

Key Points:

- A geochemical method is presented to estimate the fraction of minerals dissolved, altered, and residual after various weathering degrees.
- The method, calibrated to mineralogical observations, improves the accuracy and precision of source to sink mass-balance evaluations.
- The method is illustrated with an example and documented with an Excel workbook available for download.

Abstract

Evaluation of the approximate magnitude of the gross discrepancy between the volume of sediment produced on the hinterland and the volume deposited in the basin, over long time and length scales, is required to make source-to-sink sediment mass-balance calculations more accurate so that multiple sources for a single widespread stratigraphic unit, or bypass of the unit, might be more easily detected.

This paper outlines a method to characterize the sources of sediments, or provenance lithotypes, according to their relative ability to produce dissolved ions, clay minerals, and unaltered residue at different levels of weathering. Estimating the relative proportion of the hinterland that is dissolved supports mass-balance analysis comparing hinterland denudation with basinal deposition, whereas estimating the relative proportion of clay (both original clay, eroded from mudstone, for example, as well as newly created clay produced by weathering of feldspar) supports potential identification of multiple sediment sources. The method is illustrated with a practical example from the Bohemian Massif and documented with an Excel workbook.

This is a mineralogical approach based on mineral inventories of weathering profiles. Even if the prediction is necessarily uncertain because the mineralogical representation of the PLs are gross abstractions, the modelled transformation processes are crude cartoons, and the extent of transformation under different environmental conditions is wild speculation based on sparse examples, quantitative provenance analysis will be more accurate and more precise than it would be if dissolution and alteration were not explicitly accounted. There is ample opportunity for the community to improve the procedure!

Plain Language Summary

Estimating the fraction of material that is dissolved, altered to new materials, or remains as unaltered residue when rocks weather at the Earth's surface supports mass-balance analysis of sedimentary systems from source to sink. Mass-balance analysis help determine if sediments in a specific sediment body came from a single source or many sources, or if some sediments from potential sources has bypassed the deposit entirely. Knowing the source of sediment can help predict the physical properties of sediments even when they cannot be observed directly. This paper outlines a method for the estimation, provides a worked example from the Bohemian Massif, and supplies an Excel workbook to implement the estimation.

1 INTRODUCTION

1.1 Motivation

In resource exploration, it is often necessary to guess the physical properties of a sandstone body that cannot be directly observed, anything from the porosity and permeability of a potential hydrocarbon reservoir in a frontier basin with no wells for 100s of km (Ebner 2006), to the compressive strength of a potential bluestone deposit between quarries a few km apart (DePalma 2008). The financial stakes can be hundreds of millions of dollars for a deep-water well, or hundreds of dollars for a mining permit, but explorers need assurance that the potential resource is worth the expenditure. Often it is not necessary to be exactly right, but it is highly desirable not to be dramatically wrong.

One approach to physical-property estimation is forward modelling of sandstone diagenesis (Taylor et al. 2022), which combines an estimate of sand composition and texture at deposition, with the effective-stress/temperature/time history of the deposit after burial, to calculate the diagenetic processes and physical-property modifications that could have occurred. The estimate of sand composition and texture at deposition can be formally predicted with a tool like the Sand Generation and Evolution Model (SandGEM) (Heins & Kairo 2007, Kairo et al. 2010). Alternatively, the genetic principles of SandGEM can guide a systematic search for modern or ancient analogue sand(stone) with similar genetic context and similar burial-thermal history that could therefore be expected to demonstrate similar physical properties.

This paper outlines a procedure to characterize the sources of sediments, or provenance lithotypes (PL) according to their relative ability to produce dissolved ions, clay minerals, and unaltered residue at different levels of weathering, which is a useful step in estimating the depositional composition and texture of sediments that cannot be easily observed. Estimating the relative proportion of the hinterland that is dissolved supports mass-balance analysis comparing hinterland denudation with basinal deposition, whereas estimating the relative proportion of clay (both original clay, eroded from mudstone, for example, as well as newly created clay produced by weathering of feldspar) supports potential identification of multiple sediment sources (Heins 2023).

This is a mineralogical approach based on mineral inventories of weathering profiles that directly capture in situ interactions of the lithosphere, hydrosphere, and atmosphere. These methods have been previously outlined in Brengman et al. (2016), and first applied in public by Heins (2023). The calculations described in this paper are formalized in an Excel spreadsheet that is available for download as supplemental material. Although the approach might possibly aid more sophisticated evaluation of Sediment Routing Systems (Allen 2008, Allen 2017) or for Quantitative Provenance Analysis (Weltje and von Eynatten 2004, Weltje 2012, Caracciolo 2020), as discussed at the end of the paper, this is primarily a blunt tool to help make pragmatic exploration judgements that are unlikely to be dramatically wrong, because the judgements honour fundamental mineralogical and chemical principles.

1.2 Conceptual Framework

1.2.1 Raw Materials and Products

Not all the material removed from a source area will arrive in the sink as solids, and not all of the solids will be the same mineralogy as the original Provenance Lithotypes (PL) (Figure 1). Some fraction of the PL will have been dissolved (D) to ions, which leave the system in solution and cannot be tracked individually. Another fraction of the PL will be altered (A) to new minerals by the removal of the dissolved ions, for example plagioclase feldspars to various clay minerals. The residue (R) that has not been dissolved or altered consists of disintegrated original material with a different bulk mineralogy and chemical composition from the PL. The degree of alteration can be quantified by comparing the bulk chemical composition of the new minerals plus the unaltered residue to the bulk chemical composition of the original PL, for example using the Chemical Index of Alteration (CIA) introduced by Nesbitt & Young (1982). We do not advocate CIA for any other purpose than the conceptual comparison of parent material to daughter weathering products in the thought experiment where the entire volume of daughter products can be quantified; in practice it is rarely possible to ensure that a natural sample fully captures all daughter products (Weltje et al. 1998, Garzanti & Resentini 2016, Hatzenbühler et al. 2022).

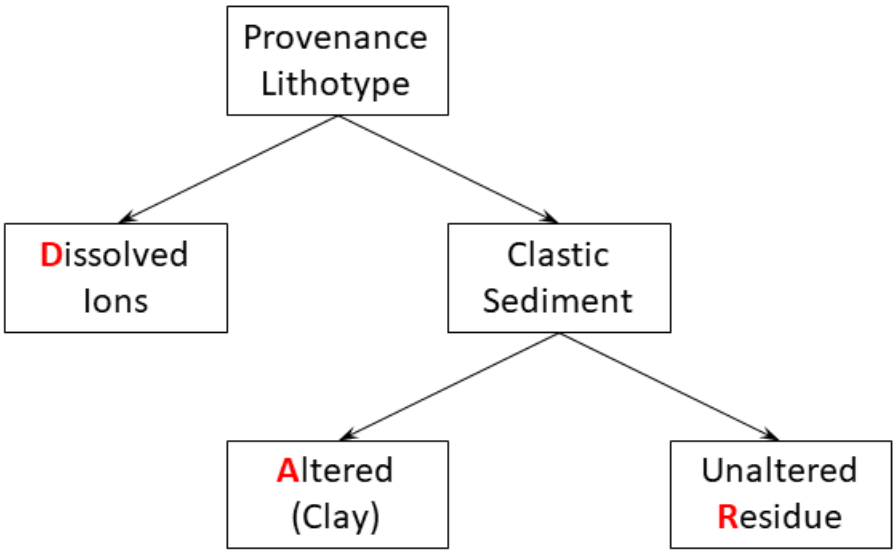

Figure 1– Partitioning of products from the breakdown of a single Provenance Lithotype

1.2.2 Procedure

We estimate the relative proportion of dissolved, altered, and residual material produced by weathering a defined roster of common rock types using geochemical mass balance. The procedure can be generalized to any provenance lithotype. We refer to the procedure by the acronym DARE (Dissolution, Alteration, and Residue Estimator).

1.2.3 Scale

The typical object of analysis will be several hundred meters to a few km of rock (102-103 m) removed from thousands to tens of thousands of square kilometers (103-104 km2) of landscape during hundreds of thousands to millions of years (105-106 years). Bookkeeping is done within a Lagrangian framework (Section 9.3 of Weltje 2012), in which we consider together all the residue, altered minerals, and dissolved ions that were derived from an originally contiguous volume of parent rock, regardless of where the individual bits have migrated in space. The altered and residual materials certainly will not all be deposited in the same place at the time (Castelltort & Van Den Driessche 2003, Allen 2008, Romans et al. 2016, Toby et al. 2019, Caracciolo 2020) because different parts of the landscape will produce sediments at different rates, the sediments will leave the landscape at different rates, and travel to the basin by different routes, and at different rates, according to the morphology of the landscape and the hydrodynamics of different kinds of particles; in the basin the material will be segregated into different depositional environments. Nevertheless, over the intended time and length scale, in many kinds of basins, a meaningful fraction of the original sediment generated on the hinterland will be deposited as sediment bodies large enough to serve as economically meaningful reservoirs (for hydrocarbons, or geothermal fluids, or captured carbon dioxide, for example): 102-103 m thick covering 103-104 km2. DARE is intended to address the approximate magnitude of the gross discrepancy between the volume of sediment produced on the hinterland and the volume deposited in the basin, to make mass-balance calculations more accurate so that multiple sources for a single deposit, or bypass of the deposit, might be more easily detected (Heins 2023). Application of this procedure to smaller spatial scales, or to shorter time scales, or to other analytic requirements may not produce meaningful results (Heins & Bailey 2020, see also the Discussion and Conclusion section).

1.2.4 Relative Uncertainty

The relative proportion of Dissolved (D), Altered (A), and Residual (R) components is one of the least uncertain elements in a sediment mass-balance analysis. D + A + R must add up to the total material removed from the landscape, which almost always is the most uncertain element. Imprecision in partitioning the denuded volume into the three elements for a given PL pales into insignificance in comparison to the uncertainty in defining the denuded volume and inaccuracy in quantifying it.

For example, in the study of Barnes & Heins (2007), which constitutes a well-constrained example, the uncertainty in the volume denuded from the Bolivian Andes during part of the Miocene encompassed three variables:

1. the size of the drainage area (somewhere between 100,000 and 153,000 km2);
2. the average rate of vertical incision (0.1-0.4 mm/year = km/Ma)
3. the duration of incision (2.1 ± 0.2 Ma)

The contrast between the smallest convolution (19,000 km3) and the largest convolution (141,000 km3) of these three factors is 7.4x.

By comparison, 1000 cm3 of fresh granodiorite weathered to its final, chemically stable, mineral assemblage would:

- dissolve 352 cm3

- alter 376 cm3 to clay
- retain 272 cm3 of unaltered residue (mostly quartz with traces of heavy minerals).

This represents a contrast between maximum and minimum values (no weathering vs maximal weathering) of 1.5x = 1000/(376+272) for the total mass of solid material, and 2.4x = (376+272)/272 for the proportion of altered material in the solids.

In most of the practical cases we have examined, the relative uncertainty in the denuded volume is even bigger than the special case of the Bolivian Andes, due to the uncertain location of ancient drainage divides (Markwick & Valdes 2004) and the inherent difficulty of converting imprecise point estimates of vertical incision into accurate rates of areal denudation (Barnes & Heins 2007, Sadler & Jerolmack 2014, Heins & Bailey, 2020)

The uncertainty in the solid yield and the fraction of alteration within the solids typically is even smaller than the granodiorite example above because the degree of alteration is rarely maximal and the PL assemblage tends to include (or even be dominated by) rocks that have a smaller content of labile minerals than granodiorite (for example quartzose sandstone).

Estimates of the relative proportion of different PL on the landscape are also uncertain, even on modern Earth (let alone projected into the past), given the vagaries of geologic mapping, especially at smaller scales (Dürr et al. 2005, Hartmann & Moosdorf 2012, Börker et al. 2018). Since the estimates for any single PL are reasonable and directionally correct, inaccuracies in the landscape-averaged values for D, A, and R will tend to be attenuated by the uncertainties in relative mix of all the PLs, rather than accentuated by that uncertainty.

1.3 Value of the Process

The values for D, A, and R calculated by the method reported below are not unreasonable (for example limestone can be dissolved almost completely at maximal alteration, quartz sandstone hardly at all) and directionally correct (for example gabbro produces more clay than granodiorite). At the same time, the values are bound to be wrong in detail because the mineralogical representation of the PLs are gross abstractions (Heins & Kairo 2007), the modelled alteration processes are crude cartoons (Velbel 1984), and the extent of alteration under different environmental conditions is wild speculation based on sparse examples (Nesbitt & Wilson 1992; Nesbitt & Markovics, 1997).

Nevertheless, using values calculated by this method in mass-balance calculations will yield better results than if dissolution and alteration were not accounted for, and the relative errors introduced will be very small compared to other uncertainties in the calculation (Heins 2023). Any of the specific factors presented in this paper easily can be modified by the interested user to reflect local conditions ± superior calibration data ± better reaction equations. We offer these values and this methodology as a starting point that can and should be improved by subsequent research.

2 PROCEDURE

2.1 Workflow

The general procedure to estimate the relative proportion of D, A, and R from a landscape consists of eight discrete steps, which will be presented in greater detail in subsequent sections of the paper. Any or all these steps can be improved or refined by additional investigation by the interested reader.

1. Specify a short list of provenance lithotypes that can reasonably represent an adequate fraction of the hinterland.
2. Specify a short list of idealized minerals and glasses that can reasonably represent an adequate fraction of the PL.
3. Assign an idealized mineralogic composition for each PL from the list of minerals.
4. Identify the daughter weathering products for each of the minerals.
5. Establish a small number of discrete, qualitative, weathering steps between the end members of "no alteration" to "maximum possible alteration".
6. Quantify the volumetric proportion of parent mineral altered (alteration index) at each step, and the volume reduction from the parent to the daughter.
7. Calculate the volume of remaining altered and unaltered material for each mineral (or glass), at each weathering step.
8. Integrate the values for each mineral (or glass), at each weathering step, weighted by the composition of each provenance lithotype.

2.1.1 Specify Provenance Lithotypes

A Provenance Lithotype encompasses all rocks of similar mineralogy and texture that tend to generate the same volume and character (mineralogy and texture) of sediments when subjected to a given level of alteration (Heins & Kairo 2007). Heins & Kairo 2007 identified a global list of 21 different PL (Table 1). Dürr et al. 2005 suggest a global list of 15 types (including water and ice). Hartmann & Moosdorf 2012 suggest a high-level division of 16 classes (including unconsolidated sediments) with two optional modifiers with 12 and 14 values, respectively. Börker et al. 2018 expand on the recognition of Hartmann & Moosdorf 2012 that unconsolidated sediments are in many cases the most important PL and refines the classification of those deposits.

For this paper we adopt the convention of Heins & Kairo 2007, but practical experience shows this list is deficient in the roster of metamorphic rocks, which should be expanded to address the wide range of metamorphic textures and mineralogies among rocks typically lumped together in "Precambrian shields" or other poorly resolved areas of quartzo-feldspathic crystalline basement.

The roster of sedimentary rocks is probably adequate, but care must be taken when inferring the relative abundance of "sandstone", "mudstone", and "carbonate" in mapped sedimentary units. Very often the relative abundance of fine-grained rocks is under-reported or under-appreciated in map units designated as "sand" or "sandstone", and the carbonate content of "shales" or "mudstones" is often underappreciated: famous mudrocks like the Posidonienschiefer of Germany or the Eagle Ford Shale of Texas are one-third to two-thirds carbonate.

Table 1– Example List of Provenance Lithotypes

Code	Clan	Variant	Variety	Comment
P1	Plutonic	Ultrabasic		
P2	Plutonic	Basic	Gabbro	Na-plagioclase dominant
P3	Plutonic	Basic	Diorite	Ca-plagioclase dominant
P4	Plutonic	Intermediate		
P5	Plutonic	Silicic		
P6	Plutonic	Sodic	Anorthosite	
P7	Plutonic	Potassic	Syenite	
V1	Volcanic	Basic		
V2	Volcanic	Intermediate		
V3	Volcanic	Silicic		
S1	Sedimentary	Sandstone	Quartz-rich	
S2	Sedimentary	Sandstone	Feldspar-rich	
S3	Sedimentary	Sandstone	Lithic-rich	
S4	Sedimentary	Mudstone		
S5	Sedimentary	Carbonate		
M1	Metamorphic	Metasandstone		
M2	Metamorphic	Slate		
M3	Metamorphic	Metacarbonate		
M4	Metamorphic	Schist/phyllite		
M5	Metamorphic	Gneiss	Plagioclase-rich	
M6	Metamorphic	Gneiss	K-feldspar-rich	

2.1.2 Specify Minerals

The mineral list must be long enough to capture the essential weathering behavior of all the PLs, but short enough to be tractable (Table 2). Whole categories of minerals like pyroxenes, amphiboles, micas, and clays are necessarily collapsed into one or a few representatives that stand in as idealized abstractions for the broader category to simplify the analysis. Especially for the clays we acknowledge that we have grossly oversimplified to make computations tractable. Each mineral in the table has been abstracted to typical chemistry (Stoch & Sikora 1976, Schroeder et al. 2000, van der Weijden & Pacheco 2003) that can be used for quantitative weathering calculations, and still plausibly stand in for the range of variation in nature.

The minerals in Table 2 are listed approximately in their order of weathering susceptibility as integrated from Nesbitt & Wilson 1992, Lasaga et al. 1994, Nesbitt & Markovics 1997, Railsback 2007, and Brantley 2008.

The list of Table 2 and the specified compositions have the added advantage that they provide suitable targets for the linear algebra method (Nesbitt et al. 1996, Nesbitt & Markovics 1997) for inverting modal mineralogy from major oxide compositions of PL. Apatite is listed among the minerals primarily to account for P_2O_5; apatite typically is not abundant enough to make any difference in mass balance calculations. Garnets are excluded from the list because they are rarely abundant enough in rocks to make a discernible difference in mass balance calculations. The molar mass reported in Table 2 is calculated from the given chemical formula. The molar volume is calculated from the reported molar

mass and the reported typical density. References are provided for both the formulae and the densities.

2.1.3 Assign Minerals to Provenance Lithotypes

The minerals listed in Table 2 are sufficient to describe the provenance lithotypes listed in Table 1 completely, as outlined in Table 3 and Table 4. Typical major oxide compositions of the Provenance Lithotypes from Table 1 are provided in Table 5 (after Heins & Kairo 2007). The reported mineralogic and chemical compositions are intended only as convenient abstractions for a typical representative of each rock type to ease subsequent calculations. The interested reader is encouraged to use different values that may more accurately represent specific circumstances.

2.1.4 Weathering Products of Minerals

The rock-forming minerals or glasses of Table 2 lose mass and volume as they alter into another mineral (usually a clay) or dissolve completely. The daughter products and associated fractional volume loss during alteration are calculated in Table 6, for minerals, and in Table 7, for glasses. Apatite and calcite are not included in the list because they are considered to dissolve completely without solid daughter products; kaolinite, quartz, rutile, and hematite are not included because they are considered fully resistant to alteration (although these assumptions are not strictly true in real life). Treating apatite as a highly labile minerals rests on the very high dissolution rates reported by Brantley 2008, Figure 5.1. Obviously, apatite is common as a detrital component in sandstones, and even has special value as a provenance indicator (O'Sullivan et al. 2020). It would be equally legitimate to include apatite among the refractory minerals, like quartz, that are assumed not to dissolve at all. Both decisions have no practical impact as apatite is rarely if ever abundant enough in the PL to make a discernible difference in a mass-balance calculation; apatite is included in the mineral list primarily to accommodate P2O5 when inverting oxide geochemistry to mineralogy.

The parent minerals or glasses and daughter weathering products present in Table 6 are idealized end members of illustrative sequences that can only vaguely approximate the complexity of nature. The precise definitions of the daughter weathering products are chosen to simplify calculations. The interested reader is encouraged to use different values that may more accurately represent specific circumstances.

Table 2 – Example List of Minerals and Glasses

Mineral or Glass	Representative Chemical Formula	Molar mass (g)	Typical Density (g/cm^3)	Molar volume (cm^3)	Composition Reference	Density Reference
Apatite	$(CaO)_5(PO_4)_3$	565.3	3.20	176.7	1	1
Calcite	$CaCO_3$	100.1	2.71	36.9	1	1
Pyroxene	$CaMg_{0.7}Fe_{0.3}Al_{0.2}Si_{1.8}O_{5.9}$	224.2	3.50	64.1	2	1
Plagioclase (An_{100})	$CaAl_2Si_2O_8$	278.2	2.76	100.8	2	1
Olivine	$Mg_{1.5}Fe_{0.5}SiO_4$	156.5	3.51	44.5	2	1
Basaltic glass	same as V1 (**Error! Reference source not found.**) major oxide wt%		2.77			3
Andesitic glass	same as V2 (**Error! Reference source not found.**) major oxide wt%		2.47			3
Rhyolitic glass	same as V3 (**Error! Reference source not found.**) major oxide wt%		2.37			3
Biotite	$KMg_3AlSi_3O_{10}(OH)_2$	417.3	3.00	139.1	4	1
Hornblende	$Na_{0.45}Ca_{1.90}Mg_{2.33}Fe^{2+}_{1.98}Al_{0.80}Si_{6.53}Al_{1.45}Ti_{0.02}O_{22}(OH)_2$	884.8	3.24	273.5	5	1
Plagioclase (An_{70})	$Na_{0.3}Ca_{0.7}Al_{1.7}Si_{2.3}O_8$	273.4	2.72	100.5	2	1
Plagioclase (An_0)	$NaAlSi_3O_8$	262.2	2.63	99.7	2	1
K-feldspar	$KAlSi_3O_8$	278.3	2.55	109.1	1	1
Muscovite	$KAl_2Si_3AlO_{10}(OH)_2$	398.3	2.83	141.0	4	1
Vermiculite	$Mg_{0.35}Fe_{0.3}Al_2Si_{3.6}O_{11}$	356.3	2.40	148.5	4	1
Illite	$K_{0.75}Al_{2.75}Si_{3.25}O_{10}(OH)_2$	388.8	2.75	141.4	4	1
Kaolinite	$Al_2Si_2O_5(OH)_4$	258.2	2.60	99.3	4	1
Quartz	SiO_2	60.1	2.33	25.8	1	1
Rutile	TiO_2	79.9	4.90	16.3	1	1
Hematite	Fe_2O_3	159.7	5.26	30.4	1	1

References:

1. Phillips & Griffin 1981
2. van der Weijden & Pacheco 2003
3. Wohletz & Heiken 1992

4. Stoch & Sikora 1976
5. Schroeder *et al.* 2000

Table 3 – Typical Mineralogy of Plutonic and Volcanic Provenance Lithotypes

	P1	**P2**	**P3**	**P4**	**P5**	**P6**	**P7**	**V1**	**V2**	**V3**
Apatite	0.010	0.005	0.016	0.023	0.010	0.000	0.020	0.004	0.003	0.001
Calcite	0.000	0.000	0.000	0.000	0.000	0.000	0.000	0.000	0.000	0.000
Pyroxene	0.263	0.198	0.189	0.000	0.000	0.050	0.000	0.132	0.000	0.000
Plagioclase (An_{100})	0.120	0.615	0.606	0.000	0.000	0.000	0.000	0.000	0.000	0.000
Olivine	0.548	0.151	0.167	0.000	0.000	0.040	0.000	0.117	0.000	0.000
Basaltic glass	0.000	0.000	0.000	0.000	0.000	0.000	0.000	0.300	0.000	0.000
Andesitic glass	0.000	0.000	0.000	0.000	0.000	0.000	0.000	0.000	0.300	0.000
Rhyolitic glass	0.000	0.000	0.000	0.000	0.000	0.000	0.000	0.000	0.000	0.300
Biotite	0.000	0.000	0.000	0.056	0.070	0.000	0.080	0.000	0.011	0.026
Hornblende	0.000	0.000	0.000	0.024	0.000	0.000	0.000	0.000	0.092	0.000
Plagioclase (An_{70})	0.000	0.000	0.000	0.153	0.150	0.900	0.000	0.000	0.187	0.037
Plagioclase (An_{0})	0.000	0.000	0.000	0.319	0.260	0.000	0.150	0.262	0.211	0.185
K-feldspar	0.000	0.000	0.000	0.175	0.150	0.000	0.680	0.163	0.054	0.230
Muscovite	0.000	0.000	0.000	0.000	0.000	0.000	0.000	0.000	0.000	0.000
Vermiculite	0.000	0.000	0.000	0.000	0.000	0.000	0.000	0.000	0.000	0.000
Illite	0.000	0.000	0.000	0.000	0.000	0.000	0.000	0.000	0.000	0.000
Kaolinite	0.000	0.000	0.000	0.000	0.000	0.000	0.000	0.000	0.000	0.000
Quartz	0.000	0.000	0.000	0.247	0.350	0.000	0.050	0.000	0.142	0.220
Rutile	0.034	0.016	0.015	0.000	0.000	0.010	0.000	0.011	0.000	0.000
Hematite	0.026	0.015	0.006	0.001	0.010	0.000	0.020	0.011	0.000	0.000

Table 4 – Typical Mineralogy of Sedimentary and Metamorphic Provenance Lithotypes

	S1	**S2**	**S3**	**S4**	**S5**	**M1**	**M2**	**M3**	**M4**	**M5**	**M6**
Apatite	0.000	0.000	0.000	0.000	0.000	0.000	0.000	0.000	0.000	0.000	0.000
Calcite	0.010	0.050	0.100	0.045	0.750	0.000	0.030	0.750	0.000	0.000	0.000
Pyroxene	0.000	0.000	0.000	0.000	0.000	0.000	0.000	0.000	0.000	0.000	0.000
Plagioclase (An_{100})	0.000	0.000	0.000	0.000	0.000	0.000	0.000	0.000	0.000	0.000	0.000
Olivine	0.000	0.000	0.000	0.000	0.000	0.000	0.000	0.000	0.000	0.000	0.000
Basaltic glass	0.000	0.000	0.000	0.000	0.000	0.000	0.000	0.000	0.000	0.000	0.000
Andesitic glass	0.000	0.000	0.000	0.000	0.000	0.000	0.000	0.000	0.000	0.000	0.000
Rhyolitic glass	0.000	0.000	0.000	0.000	0.000	0.000	0.000	0.000	0.000	0.000	0.000
Biotite	0.013	0.050	0.100	0.000	0.000	0.050	0.000	0.000	0.325	0.006	0.060
Hornblende	0.000	0.000	0.000	0.000	0.000	0.000	0.000	0.000	0.000	0.000	0.000
Plagioclase (An_{70})	0.010	0.094	0.063	0.000	0.010	0.000	0.000	0.010	0.000	0.000	0.004
Plagioclase (An_{0})	0.035	0.094	0.063	0.010	0.010	0.150	0.030	0.010	0.050	0.325	0.083
K-feldspar	0.045	0.188	0.125	0.030	0.010	0.150	0.010	0.010	0.050	0.175	0.413
Muscovite	0.000	0.000	0.000	0.000	0.000	0.000	0.000	0.000	0.325	0.095	0.040
Vermiculite	0.000	0.000	0.000	0.183	0.000	0.000	0.210	0.000	0.000	0.000	0.000
Illite	0.000	0.000	0.000	0.366	0.000	0.000	0.300	0.000	0.000	0.000	0.000
Kaolinite	0.000	0.000	0.000	0.061	0.050	0.000	0.100	0.050	0.000	0.000	0.000
Quartz	0.875	0.475	0.450	0.300	0.150	0.550	0.300	0.150	0.050	0.250	0.250
Rutile	0.013	0.050	0.100	0.005	0.020	0.050	0.010	0.010	0.180	0.140	0.140
Hematite	0.000	0.000	0.000	0.000	0.000	0.050	0.010	0.010	0.020	0.010	0.010

Table 5 – Major Element Oxide Composition of Provenance Lithotypes

PL	SiO2	TiO2	Al203	Fe2O3	FeO	MnO	MgO	CaO	Na2O	K2O	H2O	P2O5	
P1	43.54	0.81	3.99	2.51	9.84	0.21	34.02	3.46	0.56	0.25	0.76	0.05	Table 48, “Peridotite”
P2	48.36	1.32	16.81	2.55	7.92	0.18	8.06	11.07	2.26	0.56	0.64	0.24	Table 47, “Gabbros”
P3	51.86	1.50	16.40	2.73	6.97	0.18	6.12	8.40	3.36	1.33	0.80	0.35	Table 46, “Diorites”
P4	66.80	0.57	15.66	1.33	2.59	0.07	1.57	3.56	3.84	3.07	0.65	0.21	Table 45, “Granodiorites”
P5	72.08	0.37	13.86	0.86	1.67	0.06	0.52	1.33	3.08	5.46	0.53	0.18	Table 45, “Granites”
P6	54.54	0.52	25.72	0.83	1.46	0.02	0.83	9.62	4.66	1.06	0.63	0.11	Table 48, “Anorthosites”
P7	59.41	0.83	17.12	2.19	2.83	0.08	2.02	4.06	3.92	6.53	0.63	0.38	Table 46, “Syenites”
V1	50.83	2.03	14.07	2.88	9.00	0.18	6.34	10.42	2.23	0.82	0.91	0.23	Table 47, “Tholeiitic basalts"
V2	54.20	1.31	17.17	3.48	5.49	0.15	4.36	7.92	3.67	1.11	0.86	0.28	Table 46, “Andesites”
V3	73.66	0.22	13.45	1.25	0.75	0.03	0.32	1.13	2.99	5.35	0.78	0.07	Table 45, “Rhyolites”
S1	78.70	0.25	4.80	1.10	0.30	0.03	1.20	5.50	0.45	0.30	1.30	0.08	Table 87, “Sandstones”
S2	70.00	0.58	8.20	2.50	1.50	0.06	1.90	4.30	0.58	2.10	3.00	0.10	Table 87, “Sandstones from platforms"
S3	66.70	0.60	13.50	1.60	3.50	0.10	2.10	2.50	2.90	2.00	2.40	0.20	Table 87, “Graywackes”
S4	58.90	0.78	16.70	2.80	3.70	0.09	2.60	2.20	1.60	3.60	5.00	0.16	Table 87, “Shales mainly from geosynclines"
S5	8.20	0.00	2.20	1.00	0.68	0.07	7.70	40.50	0.00	0.00	0.00	0.07	Table 87, “Carbonate rocks"
M1	78.70	0.25	4.80	1.10	0.30	0.03	1.20	5.50	0.45	0.30	1.30	0.08	Table 87, “Sandstones”
M2	58.90	0.78	16.70	2.80	3.70	0.09	2.60	2.20	1.60	3.60	5.00	0.16	Table 87, “Shales mainly from geosynclines"
M3	8.20	0.00	2.20	1.00	0.68	0.07	7.70	40.50	0.00	0.00	0.00	0.07	Table 87, “Carbonate rocks"
M4	62.00	1.00	19.00	2.60	4.70	0.10	2.80	1.50	2.00	3.90	0.00	0.20	Table 95, mean of "Phyllite" & "Mica schists"
M5	50.30	1.60	15.70	3.60	7.80	0.20	7.00	9.50	2.90	1.10	0.00	0.30	Table 95, “Amphibolites”
M6	70.70	0.50	14.50	1.60	2.00	0.10	1.20	2.20	3.20	3.80	0.00	0.20	Table 95, “Quartzofeldspathic gneisses"

Reference – Clark 1982

Table 6 – Parents & Daughters, Minerals

Parent Mineral or Glass	Ultimate Daughter	Molar volume of parent (cm^3)	Moles of parent to make 1 mole daughter (#/#)	Volume of parent to make 1 mole daughter (cm^3)	Molar volume of daughter (cm^3)	Fractional Volume reduction	Stoichiometry Reference
Pyroxene	Vermiculite	64.1	10.2	653.3	148.5	0.773	1
Plagioclase (An_{100})	Kaolinite	100.8	1	100.8	99.3	0.015	1
Olivine	Hematite	44.5	4	178.2	30.4	0.830	1
Biotite	Kaolinite	139.1	1	139.1	99.3	0.286	2
Hornblende	Kaolinite	273.5	0.98	268.1	99.3	0.630	3
Plagioclase (An_{70})	Kaolinite	100.5	1.7	170.8	99.3	0.419	1
Plagioclase (An_0)	Kaolinite	99.7	2	199.4	99.3	0.502	1
K-feldspar	Illite	109.1	2	218.3	138.4	0.366	4
Muscovite	Kaolinite	141.0	1.33	188.0	99.3	0.472	2
Vermiculite	Kaolinite	148.5	2	296.9	99.3	0.666	3
Illite	Kaolinite	141.4	0.93	131.5	99.3	0.245	5

References:

1. van der Weijden & Pacheco 2003
2. Stoch & Sikora 1976
3. Schroeder *et al.* 2000
4. Yuan *et al.* 2019
5. Jin *et al.* 2010

Table 7 – Parents & Daughters, Glass

Parent Glass	Density (g cm^{-3})	Mass of 100 cm^3 of glass (g)	Al_2O_3 fraction (wt/wt)	Mass of Al_2O_3 in 100 cm^3 of glass (g)	Molar weight of Al_2O_3 (g/mol)	Moles of Al_2O_3 in 100 cm^3 of glass	Moles of kaolinite produced by 100 cm^3 of glass	Molar weight of kaolinite (g/mol)	Mass of kaolinite produced by 100 cm^3 of glass (g)	Density of kaolinite (g cm^{-3})	Volume of kaolinite produced by 100 cm^3 of glass (cm^3)	Fractional Volume reduction
Basaltic	2.772	277.2	0.1599	44.32	101.96	0.435	0.435	258.16	112.23	2.60	43.16	0.568
Andesitic	2.474	247.4	0.1722	42.60	101.96	0.418	0.418	258.16	107.87	2.60	41.49	0.585
Rhyolitic	2.370	237.0	0.1353	32.07	101.96	0.314	0.314	258.16	81.19	2.60	31.23	0.688

Glass Al_2O_3 content and density reference: Wohletz & Heiken 1992, Tables B.1 and B.3

2.1.5 Qualitative Weathering Steps

We follow the example of Nesbitt & Wilson 1992 in identifying four qualitative weathering categories, as outlined in Table 8: incipient, intermediate, advanced, and extreme. Each progressively higher step implies a greater alteration of the original PL, with a corresponding reduction in volume and increase in the relative proportion of altered material to unaltered residue.

The categories divide up the total possible range of outcomes, from no modification to complete modification. In the absence of suitable (Weltje et al. 1998, Garzanti & Resentini 2016, Hatzenbühler et al. 2022) residual material to estimate a Chemical Index of Alteration associated with the weathering environment, the relevant step for a given environmental context can be evaluated using the logic for the "Transport Modification Potential" node of the Sand Generation and Evolution Model (Heins & Kairo 2007): weathering pathways predicted to produce highly quartzose (Q80-90) sand from landscapes dominated by quartzo-feldspathic crystalline basement would correspond approximately to "Advanced", whereas weathering pathways predicted to produce pure quartz sand (Q100) would correspond approximately to "Extreme".

Table 8 – Weathering Steps

Qualitative Weathering State	**Description**	**Approximate Quantitative Range of Chemical Index of Alteration (CIA)**			
		Mafic		*Felsic*	
Incipient	Primary minerals like quartz, feldspar, mica, amphibole, *etc.* dominate	42	50	50	73
Intermediate	Primary minerals that can alter have mostly been replaced by secondary alteration products like smectite, vermiculite, chlorite, and illite	50	91	73	86
Advanced	Secondary minerals have mostly been replaced by kaolinite and oxides/oxyhydroxides	91	94	86	94
Extreme	No clay minerals remain, all alterable material has been reduced to oxides, oxyhydroxides, and hydroxides of Fe, Al, and Ti	94	100	94	100

2.1.6 Quantitative Mineral Alterations

At each weathering step from incipient to extreme, some fraction of the original parent material and/or the alteration products of the previous step will be altered. The fraction for each mineral can be roughly estimated using examples from observed weathering of the Baynton Basalt (Nesbitt & Wilson 1992, their Figure 2) and the Toorongo Granodiorite (Nesbitt & Markovics 1997, their Table 3). Between them, these two examples cover most of the minerals of Table 2 in this paper, as summarized in Table 9 and Table 10 below.

Table 11 summarizes the fractional volume altered (also known as the alteration index), compared to the unaltered volume, by each parent mineral at each weathering step. The values in Table 11 are derived according to the following principals:

- the values for apatite and calcite assume that these two minerals are completely dissolved with even incipient weathering;
- the values for Pyroxene, Plagioclase (An100), Olivine, and Basaltic Glass are taken directly from Table 9;
- the values for Andesitic and Rhyolitic glasses are proportional reductions from the values for Basaltic glass;
- the values for Biotite, Hornblende, Plagioclase (An70), Plagioclase (An0), and Kspar are taken directly from Table 10;
- the values for Muscovite, Vermiculite, and Illite are proportional reductions from the values for Kspar.

The values in Table 11 are intended to be directionally correct and suitable for subsequent calculations. Although they are reported to 3 decimal places, they represent highly idealized outcomes that in the end are essentially qualitative.

Table 9 – Progressive Alteration of Baynton Basalt
(Nesbitt & Wilson 1992 Figure 2)

Mineralogy	**Samples (least to most weathered)**				
	A-1 *Starting bulk volume %*	A-2 *Remaining bulk volume %*	A-4 *Remaining bulk volume %*	A-6 *Remaining bulk volume %*	A-9 *Remaining bulk volume %*
Plagioclase	39	15	0	0	0
Glass	30	25	2	0	0
Olivine	11	5	0	0	0
Pyroxene	15	5	2	0	0
Fraction of Mineral in Parent Altered at Each Step					
Plagioclase	0.000	0.615	1.000	1.000	1.000
Glass	0.000	0.167	0.933	1.000	1.000
Olivine	0.000	0.545	1.000	1.000	1.000
Pyroxene	0.000	0.667	0.867	1.000	1.000

Table 10 – Progressive Alteration of Toorongo Granodiorite
(Nesbitt & Markovics 1997 Table 3)

Mineralogy	**Samples (least to most weathered)**				
	1 *Starting bulk volume %*	4 *Remaining bulk volume %*	9 *Remaining bulk volume %*	13 *Remaining bulk volume %*	15 *Remaining bulk volume %*
Albite	29.6	28	21.8	2.8	0
Anorthite	17.3	15.8	6.9	1	0
K-feldspar *	9.6	9.2	8.7	4	0
Biotite + Chlorite	13.6	12.4	2.3	0	0
Hornblende	3.4	3.1	0.6	0	0
Fraction of Mineral in Parent Altered at Each Step					
Albite	0.000	0.054	0.264	0.905	1.000
Anorthite	0.000	0.087	0.601	0.942	1.000
K-feldspar	0.000	0.042	0.094	0.583	1.000
Biotite + Chlorite	0.000	0.088	0.831	1.000	1.000
Hornblende	0.000	0.088	0.824	1.000	1.000

* K-felspar value for sample 13 is the average of 13 and 14

Table 11 – Fraction of Each Parent Mineral Altered at Each Weathering Step

Minerals		**Alteration Index**				**Maximum Volume Reduction**
Parent	*Daughter*	*Incipient*	*Intermediate*	*Advanced*	*Extreme*	
Apatite	Solution	1.000	1.000	1.000	1.000	1.000
Calcite	Solution	1.000	1.000	1.000	1.000	1.000
Pyroxene	Vermiculite	0.667	0.867	1.000	1.000	0.773
Plagioclase (An_{100})	Kaolinite	0.615	1.000	1.000	1.000	0.015
Olivine	Hematite	0.545	1.000	1.000	1.000	0.830
Basaltic glass	Kaolinite	0.167	0.933	1.000	1.000	0.568
Andesitic glass	Kaolinite	0.143	0.800	1.000	1.000	0.585
Rhyolitic glass	Kaolinite	0.125	0.700	1.000	1.000	0.688
Biotite	Kaolinite	0.088	0.831	1.000	1.000	0.286
Hornblende	Kaolinite	0.088	0.824	1.000	1.000	0.630
Plagioclase (An_{70})	Kaolinite	0.087	0.601	0.942	1.000	0.419
Plagioclase (An_{0})	Kaolinite	0.054	0.264	0.905	1.000	0.502
K-feldspar	Illite	0.042	0.094	0.583	1.000	0.366
Muscovite	Kaolinite	0.021	0.063	0.438	1.000	0.472
Vermiculite	Kaolinite	0.017	0.056	0.438	1.000	0.666
Illite	Kaolinite	0.013	0.051	0.438	1.000	0.245
Kaolinite	Kaolinite	0.000	0.000	0.000	0.000	0.000
Quartz	Quartz	0.000	0.000	0.000	0.000	0.000
Rutile	Rutile	0.000	0.000	0.000	0.000	0.000
Hematite	Hematite	0.000	0.000	0.000	0.000	0.000

Please refer to the text for the derivation of the alteration indices.

2.2 Integrated Alteration and Volume Reduction by Provenance Lithotype and Weathering Step

Table 12 summarizes the procedure to integrate parent mineral alteration and daughter-mineral volume reduction to calculate the volume of dissolved, altered, and residual material, as well as the composition of the derived sediment, for a particular PL at a particular weathering step. The following sections describe how the values in each column of the table are calculated.

2.2.1 PL Composition

The column "PL Composition" comes from Table 3 (for igneous rocks) or Table 4 (for sedimentary or metamorphic rocks. This example uses the composition of P4, plutonic intermediate (granodiorite). The values in this column are the proportions of the original volume of each mineral to the original volume of the whole rock before weathering (v0/v0). The values do not depend on the weathering step.

2.2.2 Alteration Index

The column "Alteration Index" comes from Table 11. This example uses the values for the "Intermediate" weathering step. Each value represents the fraction of the original volume of parent mineral that will be altered to something else (dissolved ions and daughter mineral). The values do not depend on the PL, only on the weathering step.

2.2.3 Volume Reduction

The column "Volume Reduction" comes from Table 6 (for minerals) or Table 7 (for volcanic glass). This column is the same regardless of the PL or the weathering step. These values represent the volume fraction of original parent mineral lost during the creation of the daughter mineral.

2.2.4 Parent Remaining

The column "Parent Remaining" is equal to "PL Composition" x (1-"Alteration Index"). It is the volume of parent mineral left after alteration (v1), compared to the original volume of that mineral (v0). If there was no Parent present in the original rock, the value will be zero, regardless of the Alteration Index. The sum of all the values in this column represents the volumetric proportion of Residual, unaltered material (R) at the conclusion of weathering, compared to the original volume of rock.

2.2.5 Daughter Produced

The column "Daughter Produced" is equal to "PL Composition" x "Alteration Index" x (1-"Volume Reduction"). It is the volume of daughter mineral produced by the alteration, compared to the volume of the original parent that was altered. The sum of all the values in this column represents the volumetric proportion of Altered material (A) at the conclusion of weathering, compared to the original volume of rock.

2.2.6 Parent Dissolved

The column “Parent Dissolved” is equal to “PL Composition” – “Parent Remaining” – “Daughter Produced”. The sum of all the values in this column represents the volumetric proportion of Dissolved material (D) at the conclusion of weathering, compared to the original volume of rock. The sum of D + A + R must equal 1.

2.2.7 Sediment Composition

The column “Sediment Composition” is reported with respect to the clastic sediments (A + R) produced by weathering; it is the volumetric proportion of each component in the generated sediment.

- The values for all lines from “Carbonates” through “K-feldspar” are equal to the value for that line in “Parent Remaining” divided by the sum of the columns “Parent Remaining” and “Daughter Produced”.
- The values for the clay-mineral line “Vermiculite”, represents the sum of “Parent Remaining” for “Vermiculite” plus the “Daughter Produced” for “Pyroxene”, divided by the sum of the columns “Parent Remaining” and “Daughter Produced”.
- The values for the clay-mineral line “Illite” represents the sum of “Parent Remaining” for “Illite” plus the “Daughter Produced” for “K-feldspar”, divided by the sum of the columns “Parent Remaining” and “Daughter Produced”.
- The values for the clay-mineral line “Kaolinite” represents the sum of “Parent Remaining” for “Kaolinite” plus the sum of “Daughter Produced” for the three volcanic glasses, the two micas, “Hornblende”, the three plagioclase feldspars, and the two other clays, divided by the sum of the columns “Parent Remaining” and “Daughter Produced”.

The sum of the “Sediment Composition” must equal 1.

Table 12 -- Integrated Calculation of Dissolved, Altered, and Residual Volumes for One Provenance Lithotype (P4) at One Weathering Step (Intermediate)

Table 12 -- Integrated Calculation of Dissolved, Altered, and Residual Volumes for One Provenance Lithotype (P4) at One Weathering Step (Intermediate)

Minerals		**PL composition**	**Alteration Index**	**Volume Reduction**	**Parent Remaining**	**Daughter Produced**	**Parent Dissolved**	**Sediment Composition**
Parent	*Daughter*	(v_0/v_0)	(v_0/v_0)	(v_1/v_0)	(v_1/v_0)	(v_1/v_0)	(v_0/v_0)	(v_1/v_1)
Apatite	Solution	0.023	1.000	1.000	0.000	0.000	0.023	0.000
Calcite	Solution	0.000	1.000	1.000	0.000	0.000	0.000	0.000
Pyroxene	Vermiculite	0.000	0.867	0.773	0.000	0.000	0.000	0.000
Plagioclase (An_{100})	Kaolinite	0.000	1.000	0.015	0.000	0.000	0.000	0.000
Olivine	Hematite	0.000	1.000	0.830	0.000	0.000	0.000	0.000
Basaltic glass	Kaolinite	0.000	1.000	0.568	0.000	0.000	0.000	0.000
Andesitic glass	Kaolinite	0.000	1.000	0.585	0.000	0.000	0.000	0.000
Rhyolitic glass	Kaolinite	0.000	1.000	0.688	0.000	0.000	0.000	0.000
Biotite	Kaolinite	0.056	0.831	0.286	0.009	0.033	0.013	0.011
Hornblende	Kaolinite	0.024	0.824	0.630	0.004	0.007	0.012	0.005
Plagioclase (An_{70})	Kaolinite	0.153	0.601	0.419	0.061	0.053	0.039	0.071
Plagioclase (An_0)	Kaolinite	0.319	0.264	0.502	0.235	0.042	0.042	0.272
K-feldspar	Illite	0.175	0.094	0.366	0.159	0.010	0.006	0.184
Muscovite	Kaolinite	0.000	0.063	0.472	0.000	0.000	0.000	0.000
Vermiculite	Kaolinite	0.000	0.056	0.666	0.000	0.000	0.000	0.000
Illite	Kaolinite	0.000	0.051	0.245	0.000	0.000	0.000	0.012
Kaolinite	Kaolinite	0.000	0.000	0.000	0.000	0.000	0.000	0.158
Quartz	Quartz	0.247	0.000	0.000	0.247	0.000	0.000	0.286
Rutile	Rutile	0.000	0.000	0.000	0.000	0.000	0.000	0.000
Hematite	Hematite	0.001	0.000	0.000	0.001	0.000	0.000	0.001

3 Results

We have repeated the same kind of calculation reported in Table 12 for all the PL and all the weathering steps. The results are reported in Table 13, Table 14, Table 15, and Table 16. Each table summarize the results for every PL under Incipient, Intermediate, Advanced, and Extreme weathering, respectively. The tables report the partitioning of the total volume in two ways: among Dissolved, Altered, and Residual; and among Quartz, Feldspar, Clay, and Other constituents.

The values in these tables are intended to be directionally correct and convenient for sediment budget or mass balance calculations. Although they are reported to 3 decimal places, they represent highly idealized outcomes that are essentially qualitative and should be considered as gross approximations within a wide range of variation.

Table 13 – Summary Results for All PL under Incipient Weathering

PL	Short Name	Dissolved	Altered	Residual	Sum	Quartz	Feldspar	Clay	Other	Sum
P1	Peridotite	0.395	0.164	0.443	1	0.000	0.076	0.186	0.738	1
P2	Gabbro	0.181	0.417	0.402	1	0.000	0.289	0.492	0.219	1
P3	Diorite	0.195	0.411	0.393	1	0.000	0.290	0.492	0.218	1
P4	Granodiorite	0.043	0.025	0.930	1	0.259	0.638	0.026	0.077	1
P5	Granite	0.027	0.023	0.951	1	0.360	0.541	0.024	0.076	1
P6	Anorthosite	0.077	0.057	0.867	1	0.000	0.890	0.057	0.053	1
P7	Syenite	0.036	0.027	0.936	1	0.052	0.824	0.028	0.096	1
V1	Basalt	0.163	0.064	0.773	1	0.000	0.483	0.063	0.454	1
V2	Andesite	0.047	0.038	0.915	1	0.149	0.443	0.040	0.368	1
V3	Rhyolite	0.037	0.026	0.935	1	0.229	0.446	0.027	0.298	1
S1	Q sandstone	0.012	0.003	0.985	1	0.885	0.086	0.003	0.025	1
S2	Arkose	0.060	0.015	0.926	1	0.505	0.377	0.016	0.102	1
S3	Greywacke	0.108	0.014	0.877	1	0.505	0.265	0.016	0.214	1
S4	Mudstone	0.049	0.006	0.945	1	0.315	0.040	0.639	0.005	1
S5	Carbonate	0.751	0.001	0.248	1	0.602	0.113	0.205	0.080	1
M1	Metasandstone	0.008	0.011	0.981	1	0.554	0.288	0.011	0.147	1
M2	Slate	0.034	0.005	0.960	1	0.311	0.039	0.629	0.021	1
M3	Marble	0.751	0.001	0.248	1	0.602	0.113	0.205	0.080	1
M4	Schist/phyllite	0.014	0.027	0.960	1	0.051	0.097	0.027	0.826	1
M5	Gneiss, plag	0.013	0.015	0.974	1	0.253	0.481	0.015	0.251	1
M6	Gneiss, Kspar	0.011	0.018	0.972	1	0.253	0.483	0.018	0.246	1

Table 14 – Summary Results for All PL under Intermediate Weathering

PL	Short Name	Dissolved	Altered	Residual	Sum	Quartz	Feldspar	Clay	Other	Sum
P1	Peridotite	0.643	0.263	0.095	1	0.000	0.000	0.474	0.526	1
P2	Gabbro	0.272	0.671	0.057	1	0.000	0.000	0.886	0.114	1
P3	Diorite	0.290	0.663	0.046	1	0.000	0.000	0.895	0.105	1
P4	Granodiorite	0.135	0.146	0.716	1	0.286	0.527	0.170	0.017	1
P5	Granite	0.104	0.137	0.759	1	0.391	0.432	0.153	0.024	1
P6	Anorthosite	0.293	0.331	0.376	1	0.000	0.508	0.459	0.033	1
P7	Syenite	0.082	0.108	0.810	1	0.054	0.792	0.117	0.037	1
V1	Basalt	0.400	0.219	0.380	1	0.000	0.568	0.333	0.099	1
V2	Andesite	0.306	0.255	0.439	1	0.205	0.402	0.368	0.026	1
V3	Rhyolite	0.255	0.160	0.584	1	0.296	0.483	0.215	0.006	1
S1	Q sandstone	0.022	0.018	0.961	1	0.894	0.072	0.019	0.016	1
S2	Arkose	0.104	0.086	0.811	1	0.530	0.309	0.096	0.065	1
S3	Greywacke	0.152	0.097	0.751	1	0.531	0.217	0.114	0.138	1
S4	Mudstone	0.059	0.021	0.921	1	0.319	0.037	0.639	0.005	1
S5	Carbonate	0.754	0.005	0.240	1	0.610	0.083	0.225	0.081	1
M1	Metasandstone	0.037	0.058	0.905	1	0.571	0.256	0.060	0.113	1
M2	Slate	0.046	0.020	0.934	1	0.314	0.033	0.632	0.021	1
M3	Marble	0.754	0.005	0.240	1	0.610	0.083	0.225	0.081	1
M4	Schist/phyllite	0.095	0.213	0.692	1	0.055	0.091	0.235	0.619	1
M5	Gneiss, plag	0.053	0.060	0.888	1	0.264	0.420	0.063	0.253	1
M6	Gneiss, Kspar	0.042	0.074	0.885	1	0.261	0.456	0.077	0.206	1

Table 15 – Summary Results for All PL under Advanced Weathering

PL	Short Name	Dissolved	Altered	Residual	Sum	Quartz	Feldspar	Clay	Other	Sum
P1	Peridotite	0.670	0.271	0.060	1	0.000	0.000	0.537	0.463	1
P2	Gabbro	0.292	0.677	0.031	1	0.000	0.000	0.920	0.080	1
P3	Diorite	0.310	0.668	0.021	1	0.000	0.000	0.928	0.072	1
P4	Granodiorite	0.297	0.341	0.360	1	0.352	0.160	0.487	0.001	1
P5	Granite	0.239	0.305	0.456	1	0.460	0.126	0.401	0.013	1
P6	Anorthosite	0.427	0.511	0.062	1	0.000	0.091	0.880	0.029	1
P7	Syenite	0.256	0.376	0.368	1	0.067	0.400	0.506	0.027	1
V1	Basalt	0.527	0.358	0.115	1	0.000	0.196	0.715	0.089	1
V2	Andesite	0.421	0.384	0.195	1	0.245	0.092	0.663	0.000	1
V3	Rhyolite	0.363	0.301	0.335	1	0.346	0.181	0.473	0.000	1
S1	Q sandstone	0.043	0.047	0.911	1	0.914	0.024	0.049	0.014	1
S2	Arkose	0.184	0.199	0.618	1	0.582	0.113	0.244	0.061	1
S3	Greywacke	0.208	0.180	0.612	1	0.568	0.078	0.227	0.126	1
S4	Mudstone	0.148	0.163	0.688	1	0.352	0.016	0.626	0.006	1
S5	Carbonate	0.761	0.014	0.226	1	0.627	0.024	0.266	0.084	1
M1	Metasandstone	0.115	0.159	0.727	1	0.621	0.087	0.179	0.113	1
M2	Slate	0.139	0.147	0.714	1	0.348	0.008	0.620	0.023	1
M3	Marble	0.761	0.014	0.226	1	0.627	0.024	0.266	0.084	1
M4	Schist/phyllite	0.193	0.348	0.458	1	0.062	0.032	0.432	0.475	1
M5	Gneiss, plag	0.206	0.237	0.557	1	0.315	0.130	0.299	0.256	1
M6	Gneiss, Kspar	0.153	0.244	0.603	1	0.295	0.213	0.289	0.204	1

Table 16 – Summary Results for All PL under Extreme Weathering

PL	Short Name	Dissolved	Altered	Residual	Sum	Quartz	Feldspar	Clay	Other	Sum
P1	Peridotite	0.670	0.271	0.060	1	0.000	0.000	0.537	0.463	1
P2	Gabbro	0.292	0.677	0.031	1	0.000	0.000	0.920	0.080	1
P3	Diorite	0.310	0.668	0.021	1	0.000	0.000	0.928	0.072	1
P4	Granodiorite	0.342	0.408	0.248	1	0.377	0.000	0.622	0.002	1
P5	Granite	0.278	0.362	0.360	1	0.485	0.000	0.501	0.014	1
P6	Anorthosite	0.449	0.541	0.010	1	0.000	0.000	0.969	0.031	1
P7	Syenite	0.367	0.563	0.070	1	0.079	0.000	0.889	0.032	1
V1	Basalt	0.565	0.413	0.022	1	0.000	0.000	0.904	0.096	1
V2	Andesite	0.444	0.414	0.142	1	0.255	0.000	0.745	0.000	1
V3	Rhyolite	0.407	0.372	0.220	1	0.372	0.000	0.628	0.000	1
S1	Q sandstone	0.052	0.061	0.888	1	0.922	0.000	0.064	0.014	1
S2	Arkose	0.220	0.256	0.525	1	0.608	0.000	0.328	0.064	1
S3	Greywacke	0.232	0.218	0.550	1	0.586	0.000	0.284	0.130	1
S4	Mudstone	0.272	0.362	0.366	1	0.412	0.000	0.581	0.007	1
S5	Carbonate	0.763	0.017	0.220	1	0.633	0.000	0.283	0.084	1
M1	Metasandstone	0.145	0.205	0.650	1	0.643	0.000	0.240	0.117	1
M2	Slate	0.262	0.318	0.420	1	0.406	0.000	0.566	0.027	1
M3	Marble	0.763	0.017	0.220	1	0.633	0.000	0.283	0.084	1
M4	Schist/phyllite	0.290	0.460	0.250	1	0.070	0.000	0.648	0.282	1
M5	Gneiss, plag	0.274	0.327	0.400	1	0.344	0.000	0.450	0.206	1
M6	Gneiss, Kspar	0.231	0.369	0.400	1	0.325	0.000	0.480	0.195	1

4 PRACTICAL APPLICATION

4.1 Permo-Triassic Boundary, Bavaria

The Permo-Triassic boundary section to the southwest of the Bohemian Massif in Bavaria, as documented in boreholes Lindau-1 and Obernsees-1 (Figure 3), has been the subject of geological investigations to: document the sedimentological evolution of the strata (Ravidà et al. 2021a); to unravel the rate at which the sediments were delivered (Ravidà et al. 2021b); and to discern the provenance of the sediment (Caracciolo et al., 2021). All these kinds of investigations would be more precise if there were a quantitative expectation for the relative contribution of different lithologies eroded from the landscape to the sediment supply, similar to the Sand Generation Index of Palomares and Arribas (1993), but also including clays.

The cited body of work about the Bohemian Permo-Triassic, and the previous decades of geologic investigation on which it is based, demonstrate that the climate became wetter from the Permian to the Triassic, which had the effect of flushing more sediment off the landscape. However, the wetter climate also probably had the effect of increasing the fraction of landscape dissolved during denudation compared to the drier climate. There were also variations in the relative abundance of plutonic, low-grade metamorphic, and high-grade metamorphic rocks contributing to the sediment supply over time. It is certain that the dissolution of granitic, low-grade metamorphic, and high-grade metamorphic rocks did not respond in exactly same way to the increasing weathering intensity of the wetter climate: removing 10 m of each type of provenance-lithotype assemblage from 1 km2 of landscape would erode 0.1 km3 of rock, but each type would not contribute the same amount, nor the same kind, of sediment to the transport system.

The DARE approach offers a pathway to quantitatively estimate the relative contribution of each PL-assemblage under each set of weathering conditions, and to set an expectation for the gross mineralogy of each contribution. This level of constraint permits more rigorous evaluation of the relative influence of climate and provenance lithology in determining the characteristics of deposited sediments.

The example calculations below merely illustrate how the method can be applied to a subset of the hinterland geology of the Franconian Basin in Bavaria using the generalized PL descriptions provided in this paper. It is certainly possible to make a more refined analysis using customized PL descriptions tailored to specific geological formations, and to broaden the analysis to a wider spectrum of geology.

Figure 2 – Location of Boreholes Lindau-1 and Obernsees-1, which document the Permo-Triassic boundary in Bavaria

4.2 Bavarian Geologic Setting

4.2.1 The Hercynia River

The wells Lindau-1 and Obernsees-1 record fluvial deposits of a river that flowed from present-day SW to NE along a structurally defined corridor parallel to the Pfahl, Danube, and Franconian faults, with headwaters near the present-day Bavarian-Austrian border; Ravidà et al. 2021b and Caracciolo et al. 2021 dub this the Hercynia river (Figure 4).

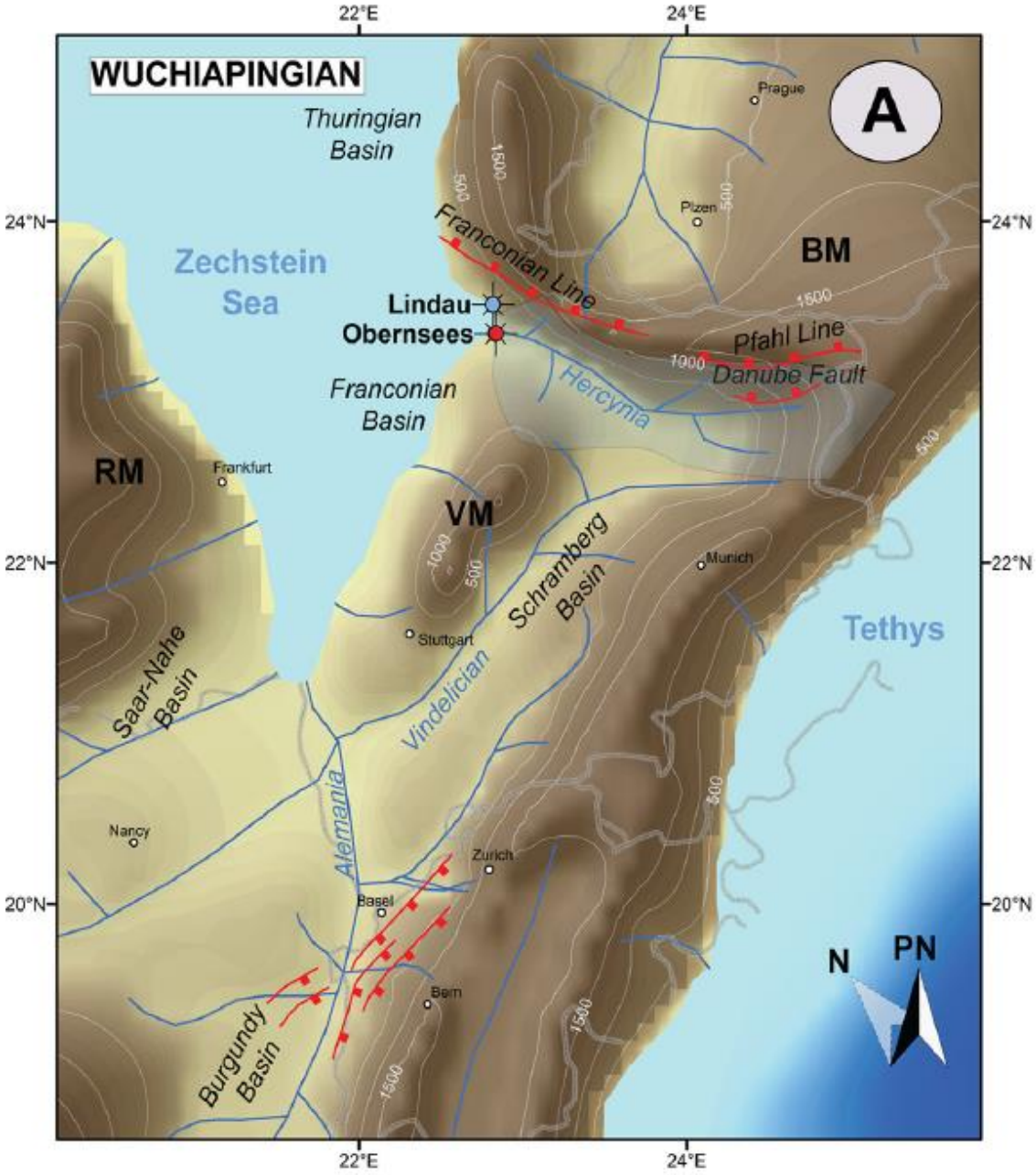

Figure 3 – Location of wells Lindau-1 and Obernsess-1 along the paleo-Hercynia River during the late Permian (after Ravidà et al. 2021b, Fig 4; paleogeography from Getech Group plc). PN = PaleoNorth; paleoelevation contours in meters; present day political boundaries rotated to paleoposition for reference.

4.2.2 Hinterland Geology

As documented by Ravidà et al. 2021a and evaluated by Caracciolo et al. 2021 (Figure 5), both metamorphic rocks of the Moldanubian Terrane, as well as Variscan granites, contributed to the sediments at Lindau and Obersees at different times.

Typical examples of both Moldanubian high-grade metamorphics and late Variscan granites are exposed today around the village of Hauzenberg, Bavaria (south of the “l” in Pfahl in Figure 5). These rocks are represented on the 1:25 000 digital geological map 7347 Hauzenberg, published by the Bayerischen Landesamt für Umwelt (https://www.lfu.bayern.de/download/geologie/dgk25/dGK25_7347_hauzenberg.pdf). Table 17 and Table 18 report the relative areal abundance of various map units from the 7347 Hauzenberg map and assign each map unit to a provenance lithotype from Table 1. Table 1 is not intended to definitively characterize any portion of the Permo-Triassic landscape of Franconia; rather it provides a modern analogue that might approximate two of the end-member geologic assemblages present on that landscape.

It should be noted that Heins & Kairo 2007 did not include amphibolite (Amfibolit in Table 18) or meta-ultramafics (Meta-Ultramafitit of Table 18) among their PL. Here we assume amphibolite to be composed primarily of amphibole and plagioclase (either calcic or sodic), which means it should be similar to either gabbro or diorite, so we consider half of the mapped amphibolite to be gabbro (P1 in Table 1) and half to be diorite (P3 in Table 1). In the same way, we treat meta-ultramafite as mineralogically equivalent to peridotite (P1 in Table 1).

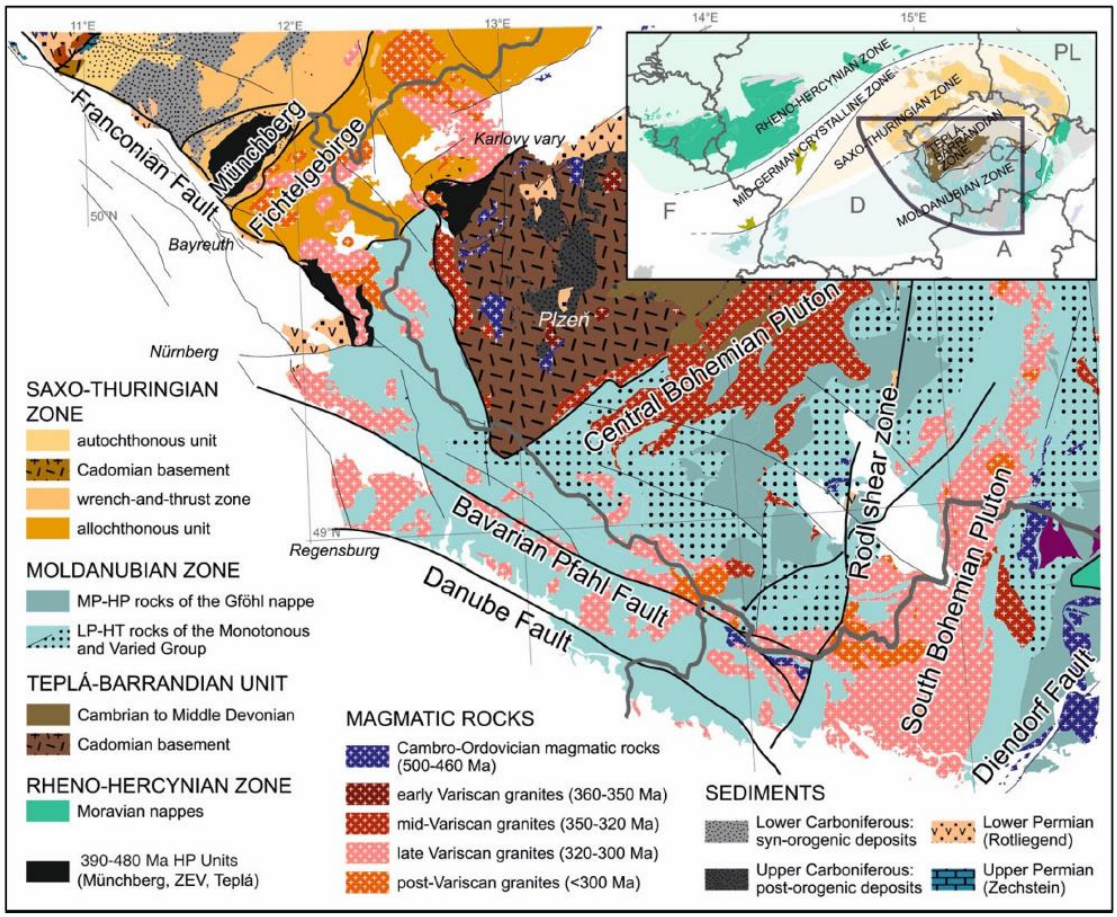

Figure 4 – Geology of the Bohemian Massif along the Bavarian-Czech Border(after Caracciolo et al. 2021, Fig. 2)

Table 17– Geological Units and Provenance Lithotypes of the Hauzenberger Pluton (HZ) and Moldanubium (MO) near Hauzenberg, Bavaria

Map Symbol	Unit Name	PL	Fraction (area/area)
HZ,Gg	Gangesteine	V3	0.01
HZ, GDr	Biotit-Granodiorit, fein- bis mittlekörnig	P4	0.24
HZ, Grf	Biotit-Muskovit-Granit, feinkörnig	P5	0.25
HZ, Grm	Biotit-Muskovit-Granit, mittlekörnig	P5	0.50
Sum			1
MO,Am	Amfibolit	P2	0.04
MO,Am	Amfibolit	P3	0.04
MO,bpGn$_{mx}$,ba	Metatektisher Biotit-Plagioklas-Gneis	M5	0.80
MO,KS	Kalksilikatgestein	M3	0.03
MO,lkGn	Leukokrater Gneis	M6	0.06
MO,mMPu	Meta-Ultramafitit	P1	0.03
Sum			1

4.3 Bavarian Application of DARE

The environmental conditions documented by Ravidà et al. 2021b range from hot and arid (Mean Annual Temperature 40°C, Mean Annual Runoff 40 mm/yr) in the mid Permian (Roadian) to cooler and wetter (33.5°C, 183 mm/yr) in the early Triassic (Induan). Using the logic of Heins & Kairo 2007, we might expect the weathering intensity in the sense of DARE to be somewhere between Incipient to Intermediate. Weighting the expected outcomes of Table 13 (Incipient) and Table 14 (Intermediate) by the expected PL abundance for the Variscan granite PL assemblage, and the Moldanubian metamorphic assemblage, we can derive an expectation for the relative magnitude of dissolution, and for the relative abundance of different minerals, across the different combinations of PL assemblage and weathering intensity (Table 19, visualized in Figure 6). Although these results are reported to 3 significant figures, they should be treated as qualitative results. Nevertheless, these qualitative results highlight subtle but important differences between provenance lithotype assemblages and weathering conditions that would not have been apparent without this systematic and quantitative analysis.

96 **Table 18 – Summary DARE output (v/v fractions) for alternate hinterland geology**

	Incipient Weathering	Intermediate Weathering
Granitic Hinterland (Hauzenberger Pluton)		
Dissolved	0.031	0.113
Altered	0.024	0.139
Residual	0.945	0.747
Sum	**1**	**1**
Quartz	0.334	0.365
Feldspar	0.563	0.455
Clay	0.024	0.157
Other	0.078	0.022
Sum	**1**	**1**
F:Q	1.69	1.25
Metamorphic Hinterland (Hauzenberger Moldanubicum)		
Dissolved	0.060	0.109
Altered	0.051	0.114
Residual	0.890	0.778
Sum	**1**	**1**
Quartz	0.236	0.245
Feldspar	0.442	0.366
Clay	0.064	0.147
Other	0.258	0.242
Sum	**1**	**1**
F:Q	1.88	1.49

97

98

99

Figure 5 – Comparison of Expected Weathering Volumes and Products

4.4 Evaluation of Bavarian Results

Changes in the volume and character of sediment delivered by the Hercynia River to the deposits at Lindau and Obernsees represent the integrated effect of changes in hinterland geology, climate, and tectonics. The integrated effect has multiple causes that must be evaluated holistically to derive proper conclusions: it is wrong to say there is a "climate signal" or a "geology signal" or a "tectonic signal". For example, a stratigraphic change from more to less feldspathic sand could be attributed either to increased weathering (intensity, due to climate ± duration, due to regional topographic gradient), or to a more granitic hinterland. If climate, topography, and exposed geology change at the same time, the effect of one may be enhanced or attenuated by the effect of the other. From the DARE results, at lower weathering, the dissolved fraction of the metamorphic assemblage is nearly twice as great as that for the granitic assemblage, whereas at higher weathering the granitic dissolved fraction is slightly more than the metamorphic one. For both assemblages the dissolved fraction increases with increasing weathering intensity, so that even though more sediment is produced at higher weathering intensity, it takes relatively more provenance lithotype to yield a fixed amount of sediment. The qualitative results of the DARE model highlight subtle but important differences between provenance lithotype assemblages and weathering conditions that would not have been apparent without this systematic and quantitative analysis.

5 DISCUSSION AND CONCLUSIONS

DARE is intended to address the approximate magnitude of the gross discrepancy between the volume of sediment produced on the hinterland and the volume deposited in the basin, over long time and length scales, to make mass-balance calculations more accurate so that multiple sources for a single widespread stratigraphic unit, or bypass of the unit, might be more easily detected (Heins 2023). DARE integrates modifications to the sediments over an entire Sediment Routing System (Allen 2008, Allen 2017) from the erosional engine, through the transfer zone, and into the long-term sink. DARE is not intended to help decipher in detail the myriad tectonic, climatic, and geomorphic perturbations that can befall the system, and which may or may not be clearly recorded in the stratigraphic record (Castelltort & Van Den Driessche 2003, Allen 2008, Romans et al. 2016, Toby et al. 2019). The challenges involved for full understanding of the entire Sediment Routing System and for a full Quantitative Provenance Analysis (Weltje and von Eynatten 2004) are well enumerated by Weltje 2012 and Caracciolo 2020; DARE is not for that purpose.

In the Bavarian example, DARE can illustrate that tectonics (in the construction of the PL assemblage) AND climate (in the intensity of weathering) AND geomorphology (in the duration and trajectory of transport) will all play a role in the original roster and ultimate modification of the minerals on the landscape. DARE can start the fundamental differentiation between the role of PL mineralogy and the integrated effect of weathering intensity and duration, but it cannot unravel the relative contribution of weathering intensity and duration, nor elucidate fine-scale stratigraphic or geographic mineralogic differences that arise from variable connectivity of different landscape elements.

DARE puts rough geochemical boundaries around the mineralogical changes that can occur across the spectrum from no alteration of a PL to the maximal alteration possible. In this sense, it might be applied to help investigate the relative ability of different PL to:

- generate dissolved ions (Allen & Allen 2013, Chapter 7.2.2);
- supply specific minerals ("mineral fertility" -- Moecher & Samson 2006, Malusà et al. 2013, Flowerdew et al. 2019, Garzanti & Andò, 2019; Chew et al. 2020); or
- supply specific size fractions (especially sand, "Sand Generation Index" – Palomares & Arribas 1993, Le Pera et al. 2001, Arribas & Tortosa 2003, Garzanti 2019).

Acknowledgments

Early versions of this manuscript benefited greatly from comments by Luca Caracciolo and Melise Harland and discussions with Meg Galsworthy and Laura Tierney.

References

Allen PA, 2008, From landscapes into geological history: Nature, v. 451, p. 274-276. https://doi.org/10.1038/nature06586

Allen PA, 2017, Sediment Routing Systems The Fate of Sediment from Source to Sink: Cambridge University Press. 407 p. https://doi.org/10.1017/9781316135754

Allen PA, Allen JR, 2013, Basin Analysis: Principles and Application to Petroleum Play Assessment, 3rd Edition: Wiley-Blackwell, ISBN 978-0-470-67377-5.

Allen PA, Armitage JJ, Carter A, Duller RA, Michael NA, Sinclair HD, Whitchurch AL, Whittaker AC, 2013, The Qs problem: sediment volumetric balance of proximal foreland basin systems: Sedimentology v. 60, p. 102–130. https://doi.org/10.1111/sed.12015

Arribas J, Tortosa A, 2003, Detrital modes in sedimenticlastic sands from low-order streams in the Iberian Range, Spain: the potential for sand generation by different sedimentary rocks: Sedimentary Geology, v. 159, p. 275-303. https://doi.org/10.1016/S0037-0738(02)00332-9

Armitage JJ, Duller RA, Whittaker AC, Allen PA, 2011, Transformation of tectonic and climatic signals from source to sedimentary archive: Nature Geoscience, v. 4, p. 231–235. https://doi.org/10.1038/ngeo1087

Armitage JJ, Dunkley Jones, T, Duller RA, Whittaker AC, Allen PA, 2013, Temporal buffering of climate-driven sediment flux cycles by transient catchment response: Earth and Planetary Science Letters, v. 369, p. 200–210. https://doi.org/10.1016/j.epsl.2013.03.020

Barnes JB, Heins, WA, 2009, Plio-Quaterary mass balance between thrust belt erosion and foreland deposition in the central Andes, southern Bolivia: Basin Research, v. 21, p. 91-109, https://doi.org/10.1111/j.1365-2117.2008.00372.x

179 Börker J, Hartmann J, Amann T, Romero-Muhalli G, 2018, Terrestrial sediments of the Earth:
180 Development of a Global Unconsolidated Sediments map database (GUM): Geochemistry,
181 Geophysics, Geosystems, v 19, p 997-1024, https://doi.org/10.1002/2017GC007273

182 Brengman LA, Heins WA, Matthews JA, 2016, Dissolution and transformation of provenance
183 lithotypes during initial sediment generation with application to play-element prediction:
184 ExxonMobil Upstream Research Company Research Application Report URC.2016.046

185 Brantley, S.L., 2008. Kinetics of Mineral Dissolution, in Kinetics of water-rock interaction,
186 Brantley, S.L., Kubicki, J.D., White, A.F. (eds): Berkeley, University of California Press,
187 Chapter 5. e-ISBN 978-0-387-73563-1

188 Caracciolo L, 2020, Sediment generation and sediment routing systems from a quantitative
189 provenance analysis perspective: review, application and future development: Earth-
190 Science Reviews, v. 209, 103226. https://doi.org/10.1016/j.earscirev.2020.103226

191 Caracciolo L, Ravidà DCG, Chew D, Janßen M, Lünsdorf, NK, Heins WA, Stephan T,
192 Stollhofen H, 2021, Reconstructing environmental signals across the Permian-Triassic
193 boundary in the SE Germanic Basin: A Quantitative Provenance Analysis (QPA) approach:
194 Global and Planetary Change, v 206, 103631,
195 https://doi.org/10.1016/j.gloplacha.2021.103631

196 Castelltort S, Van Den Driessche J, 2003, How plausible are high-frequency sediment supply-
197 driven cycles in the stratigraphic record?: Sedimentary Geology, v. 157, p. 3–13.
198 https://doi.org/10.1016/S0037-0738(03)00066-6

199 Chew D, O'Sullivan G, Caracciolo L, Mark C, Tyrrell S, 2020, Sourcing the sand: accessory
200 mineral fertility, analytical and other biases in detrital U-Pb provenance analysis: Earth-
201 Science Reviews, v. 202, 103093, https://doi.org/10.1016/j.earscirev.2020.103093

202 Clark, K.F., 1982, Mineral composition of rocks, in Carmichael, R.S., ed.,Handbook of Physical
203 Properties of Rocks, Volume 1: Boca Raton, CRC Press, p. 1–213.

204 Crovisier, J.L., Honnorez, J., Eberhart, J. P., 1987. Dissolution of basaltic glass in seawater:
205 Mechanism and rate. Geochimica et Cosmochimica Acta. Vol. 51, p. 2977-2990.
206 https://doi.org/10.1016/0016-7037(87)90371-1

207 DePalma A, 2008, Bluestone boom opens quarries to new allies, and to change: New York
208 Times, 13 May 2008, https://www.nytimes.com/2008/05/13/nyregion/13quarry.html
209 (visited 25 Jul 2023).

210 Dürr HH, Meybeck M, Dürr SH, 2005, Lithologic composition of the Earth's continental
211 surfaces derived from a new digital map emphasizing riverine material transfer: Global
212 Biogeochemical Cycles, v. 19, GB4S10 https://doi.org/10.1029/2005GB002515

213 Ebner D, 2006, Chevron risks the deep: The Globe and Mail, 30 July 2006,
214 https://www.theglobeandmail.com/report-on-business/chevron-risks-the-
215 deep/article20412515/ (visited 25 Jul 2023)

216 Fischer C, Luttge A, 2017, Beyond the conventional understanding of water-rock reactivity:
217 Earth and Planetary Science Letters, v. 457, p. 100-105.
218 https://doi.org/10.1016/j.epsl.2016.10.019

Flowerdew MJ, Fleming EJ, Morton AC, Frei D, Chew DM, Daly JS, 2019, Assessing mineral fertility and bias in sedimentary provenance studies: examples from the Barents Shelf: Geological Society, London, Special Publication 484, p. 255-274. https://doi.org/10.1144/SP484.11

Garzanti E, 2019, Petrographic classification of sand and sandstone: Earth-Science Reviews, v. 192, p. 545-563. https://doi.org/10.1016/j.earscirev.2018.12.014

Garzanti E, Andò S, 2019, Heavy mineral for junior woodchucks: Minerals, v. 9, 148, https://doi.org/10.3390/min9030148

Garzanti E, Resentini A, 2016, Provenance control on chemical indices of weathering (Taiwan river sands): Sedimentary Geology, v. 336, p. 81-95. https://doi.org/10.1016/j.sedgeo.2015.06.013

Hartmann J, Moosdorf N, 2012, The new global lithological map database GLiM: a representation of rock properties at the Earth surface: Geochemistry, Geophysics, Geosystems, v13, Q12004, https://doi.org/10.1029/2012GC004370 .

Hatzenbühler D, Caracciolo L, Weltje GJ, Praquive A, Regelous M,2022, Lithologic, geomorphic, and climatic controls on sand generation from volcanic rocks in the Sierra Nevada de Santa Marta massif (NE Colombia): Sedimentary Geology, v. 429, 106076. https://doi.org/10.1016/j.sedgeo.2021.106076

Heins WA, 1993, Source-rock texture vs. climate and topography as controls on the composition of modern, plutoniclastic sand: Geological Society of America Special Paper 284, p. 135-146. https://doi.org/10.1130/SPE284-p135

Heins WA, 2023, Honest bookkeeping for source-to-sink sediment mass-balance analysis with examples from the Angoche Margin of Mozambique and the Corsica Trough of France: Journal of Marine and Petroleum Geology, v. 153, 106265. https://doi.org/10.1016/j.marpetgeo.2023.106265

Heins WA, Bailey CH, 2020, Estimating spatially and temporally relevant denudation rates for sediment mass balance studies of hydrocarbon reservoirs: ResTech Virtual Reservoir Conference, European Association of Geoscientists and Engineers, 22 Apr 2020, https://doi.org/10.3997/2214-4609.202RESTECH07

Heins WA, Kairo S, 2007, Predicting sand character with integrated genetic analysis: Geological Society of America Special Paper 420 p 345-379. https://doi.org/10.1130/2006.2420(20)

Jin LX, Ravella R, Ketchum B, Bierman PR, Heaney P, White T, Brantley SL, 2010, Mineral weathering and elemental transport during hillslope evolution at the Susquehanna/Shale Hills Critical Zone Observatory: Geochimica et Cosmochimica Acta, v. 74, p. 3669-3691. https://doi.org/10.1016/j.gca.2010.03.036

Kairo S, Heins WA, Love KM, 2010, Predicting Sand-Grain Composition and Texture, United States Patent 7,747,552 B2, issued 29 June, 2010

Kirkman, J.,H., McHardy, W.J., 1980. A comparative study of the morphology, chemical composition and weathering of rhyolitic and andesitic glass. Clay Minerals, 15, 165-173. https://doi.org/10.1180/claymin.1980.015.2.07

Lasaga AC, Soler JM, Ganor J, Burch TE, Nagy KL, 1994, Chemical weathering rate laws and global geochemical cycles: Geochimica et Cosmochimica Acta, v58 p2361-2386. https://doi.org/10.1016/0016-7037(94)90016-7

Le Pera E, Arribas J, Critelli S, Tortosa A, 2001, The effects of source rocks and chemical weathering on the petrogenesis of siliciclastic sand from the Neto river (Calabria, Italy): implications for provenance studies: Sedimentology, v. 48, p. 357-378. https://doi.org/10.1046/j.1365-3091.2001.00368.x

Malusà MG, Carter A, Limoncelli M, Villa IM, Garzanti E, 2013, Bias in detrital zircon geochronology and thermochronometry: Chemical Geology, v. 359, p. 90-107. https://doi.org/10.1016/j.chemgeo.2013.09.016

Markwick PJ, Valdes PJ, 2004, Palaeo-digital elevation models for use as boundary conditions in coupled ocean–atmosphere GCM experiments: a Maastrichtian (late Cretaceous) example: Palaeogeography, Palaeoclimatology, Palaeoecology, v. 213, p. 37–63, https://doi.org/10.1016/j.palaeo.2004.06.015

Meister R, Robertson EC, Werre RW, Raspet R, 1980, Elastic Moduli of Rock Glasses Under pressure to 8 kBar and geophysical implications: Journal of Geophysical Research, v85 nB11 p6461-6470. https://doi.org/10.1029/JB085iB11p06461

Moecher DP, Samson SD, 2006, Differential zircon fertility of source terranes and natural bias in the detrital zircon record: implications for sedimentary provenance analysis: Earth and Planetary Science Letters, v. 247, p. 252-266. https://doi.org/10.1016/j.epsl.2006.04.035

Nesbitt, H.W., Markovics, G., 1997. Weathering of granodioritic crust, long-term storage of elements in weathering profiles and petrogenesis of siliciclastic sediments. Geochimica et Cosmochimica Acta, v. 61, no. 8, pp. 1653-1670. https://doi.org/10.1016/S0016-7037(97)00031-8

Nesbitt, H.W., Wilson, R.E., 1992. Recent chemical weathering of basalts. American Journal of Science, v. 292, p. 740-777. https://doi.org/10.2475/ajs.292.10.740

Nesbitt HW, Young GM, 1982, Early Proterozoic climates and plate motions inferred from major element chemistry of lutites: Nature, v. 299, p. 715-717. https://doi.org/10.1038/299715a0

Nesbitt HW, Young GM, McLennan SM, Keays RR, 1996, Effects of chemical weathering and sorting on the petrogenesis of siliciclastic sediments, with implications for provenance studies: Journal of Geology, v 104, p525-542. https://doi.org/10.1086/629850

Palomares M, Arribas J, 1993, Modern stream sands from compound crystalline sources: composition and sand generation index: Geological Society of America Special Paper 284, p. 313-322. https://doi.org/10.1130/SPE284-p313

Phillips WR & Griffen DT, 1981, Optical Mineralogy The Nonopaque Minerals: WH Freeman.

Poręba G, Śnieszko, Moska P, Mroczek P, Malik I, 2019, Interpretation of soil erosion in a Polish loess area using OSL, 137Cs, 210Pbex, dendrochronology and micromorphology – case study: Biedrzykowice site (S Poland): Geochronometria, v. 46, p. 57-78, https://doi.org/10.1515/geochr-2015-0109

Railsback LB, 2007, Goldich's Weathering Series explained in terms of bond strength: Some Fundamentals of Mineralogy and Geochemistry, http://railsback.org/Fundamentals/8150Goldich&BondStreng06LS.pdf

Ravidà DCG, Caracciolo L, Henares S, Janßen M, Stollhofen H, 2021a, Drainage and environmental evolution across the Permo–Triassic boundary in the south-east Germanic Basin (north-east Bavaria): Sedimentology, v69, p501-536. https://doi.org/10.1111/sed.12913

Ravidà DCG, Caracciolo L, Heins WA, Stollhofen H, 2021b, Reconstructing environmental signals across the Permian-Triassic boundary in the SE Germanic Basin: paleodrainage modelling and quantification of sediment flux: Global and Planetary Change, v206 n103632 https://doi.org/10.1016/j.gloplacha.2021.103632

Ravidà DCG, Caracciolo L, Heins WA, Stollhofen H, 2023, Towards improved discrimination and correlation of Permian-Early Triassic sediments in Central Europe: a chemostratigraphic approach: Sedimentary Geology, v 452, 106408, https://doi.org/10.1016/j.sedgeo.2023.106408

Romans BW, Castelltort S, Covault JA, Fildani A, Walsh JP, 2016, Environmental signal propagation in sedimentary systems across time scales: Earth-Science Reviews, v. 153, p. 7-29. https://doi.org/10.1016/j.earscirev.2015.07.012

Sadler PM, Jerolmack DJ, 2014, Scaling laws for aggradation, denudation and progradation rates: the case for time-scale invariance at sediment sources and sinks: Geological Society, London, Special Publication 404, Chapter 7. https://doi.org/10.1144/SP404.7

Schroeder, P.A., Melear, N.D., West, L.T., Hamilton, D.A., 2000. Meta-gabbro weathering in the Georgia Peidmont, USA: implications for globala silicate weathering rates. Chemical Geology, 163, 235-245. https://doi.org/10.1016/S0009-2541(99)00129-1

Stewart RJ, Hallet B, Zeitlar PK, Malloy MA, Allen CM, Trippett D, 2008, Brahmaputra sediment flux dominated by a highly localized rapid erosion from the easternmost Himalaya: Geology, v. 36, p. 711-714. https://doi.org/10.1130/G24890A.1

Stoch L, Sikora W, 1976, Transformation of micas in the process of kaolinitization of granites and gneisses: Clays and Clay Minerals, v. 24, p. 156-162.

Taylor TR, Lander RH, Bonnell LM, 2022. Modeling sandstone diagenesis and rock properties: Society of Economic Paleontologists and Mineralogists Concepts in Sedimentology and Paleontology 13, Chapter 12. https://doi.org/10.2110/sepmcsp.13.12

Toby SC, Duler RA, De Angelis S, Straub KM, 2019, A stratigraphic framework for the preservation and shredding of environmental signals: Geophysical Research Letters, v. 46, p. 5837-5845. https://doi.org/10.1029/2019GL082555

van der Weijden CH, Pacheco FAL, 2003, Hydrochemistry, weathering and weathering rates on Madeira Island: Journal of Hydrology, v. 283, p. 122-145. https://doi.org/10.1016/S0022-1694(03)00245-2

Velbel MA, 1984, Weathering Processes of Rock-Forming Minerals: Environmental Chemistry, Mineralogical Association of Canada Short Course Handbook, v. 10, p. 67-111.

339 Weltje GJ, 2012, Quantitative models of sediment generation and provenance: State of the art
340 and future developments: Sedimentary Geology, v. 280, p. 4-20.
341 https://doi.org/10.1016/j.sedgeo.2012.03.010

342 Weltje GJ, von Eynatten H, 2004 Quantitative provenance analysis of sediments: review and
343 outlook: Sedimentary Geology, v. 171, p. 1-11.
344 https://doi.org/10.1016/j.sedgeo.2004.05.007

345 Weltje GJ, Meijer XD, De Boer PL, 1998, Stratigraphic inversion of siliciclastic basin fills: a
346 note on the distinction between supply signals resulting from tectonic and climatic forcing:
347 Basin Research, v. 10, p. 129-153. https://doi.org/10.1046/j.1365-2117.1998.00057.x

348 Wohletz K, Heiken G, 1992, Volcanology and Geothermal Energy: Berkeley, University of
349 California Press: http://ark.cdlib.org/ark:/13030/ft6v19p151/ , Appendix B, Table B.5

350 Wolff-Boenish D, Gislason SR, Oelkers EH, Putins CV, 2004, The dissolution rates of natural
351 glasses as a function of their composition at pH4 and 10.6, and temperatures from 25 to
352 74°C: Geochimica et Cosmochimica Acta, v. 68, p. 4843-4858.
353 https://doi.org/10.1016/j.gca.2004.05.027

354 Yuan GH, Cao YC, Schultz HM, Hao F, Gluyas J, Liu KY, Yang T, Wang YZ, Xi KL, Li FL,
355 2019, A review of felspar alteration and its geological significance in sedimentary basins:
356 From shallow aquifers to deep hydrocarbon reservoirs: Earth-Science Reviews v191 p114-
357 140 Equation 25. https://www.sciencedirect.com/science/article/pii/S0012825217305512
358 .